Calorimetry

Daniel Fournier LAL-Orsay

EDIT CERN/Feb2011

<u>Calorimetric measurement</u>:

As opposed to tracking,in Calorimetry a particle of energy E is absorbed in a dense material
-the calorimeter-and a signal-that we like to be proportional to E is generated from the energy deposition.

Energy losses result from several phenomena:
  - dE/dx (ionisation, level excitation→scintillation)
  - Compton scattering
  - bremsstrahlung
  - pair production (for electrons/photons)
  - Nuclear interactions if the projectile is a pion, proton,….

+long range collective effects for charged particles propagating in matter:
  - Cerenkov radiation ($\beta c > c/n$)
  - Transition radiation (transition between 2 materials of
     different optical indices n1,n2)

1.Fundamental Phenomena

1.1 Interactions of electrons,positrons and photons with matter

Interactions of charged particles with electrons of matter

A classical treatment gives a hint of what is happening; note $1/v^2$ and log term→ there is a (flat) "minimum dE/dx" for $\gamma\beta\sim3$ ie $\beta\sim0.95$

Q,v

$\delta E= (\delta p)^2/2m_e$
$\delta P=2Qe/bv$

b

$\delta E,m_e$

db

$dS=2\pi bdb$

b

$dE/dx=4\pi\rho(N_A/A)ZQ^2/v^2e^2/m_e\int db/b$

$dE/dx=4\pi\rho(N_A/A)ZQ^2/v^2e2/m_e$ Log()

dx

Interaction of electrons and positrons with electrons of matter: **dE/dx**
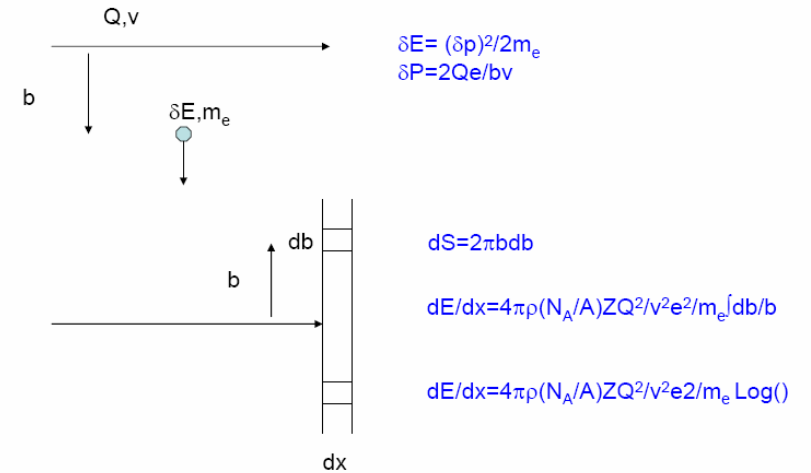
electrons

$$-\frac{dE}{dx} = k\frac{Z}{A}\frac{1}{\beta^2}\left\{\ln\frac{\gamma m_e c^2\beta\sqrt{\gamma-1}}{I\sqrt{2}} + \frac{1}{2}(1-\beta^2) - \frac{2\gamma-1}{2\gamma^2}\ln2 + \frac{1}{16}\left(\frac{\gamma-1}{\gamma}\right)^2\right\}\ (MeV/\ (g/cm^2))$$

positrons

$$-\frac{dE}{dx} = k\frac{Z}{A}\frac{1}{\beta^2}\left[\ln\frac{\gamma m_e c^2\beta\sqrt{\gamma-1}}{I\sqrt{2}} - \frac{\beta^2}{24}\left(23 + \frac{14}{\gamma+1} + \frac{10}{(\gamma+1)^2} + \frac{4}{(\gamma+1)^3}\right)\right](MeV/\ (g/cm^2)).$$

-A(Z) number of nucleons (protons) in the nuclei of the medium
- I mean excitation energy of the medium: often approximated by $16\ Z^{0.9}$eV
- k=$4\pi N_A r_e^2 m_e c^2$= 0.3071 MeV/(g/cm^2)
- N_A Avogadro number
- $r_e = \frac{1}{4\pi\varepsilon_0}\cdot\frac{e^2}{m_e c^2} = 2.818\ 10^{-15}$ m   classical radius of the electron.

For positrons : <u>add the annihilation cross section</u> $\sigma_{an}=Z\pi\, r_e^2/\gamma$ for $\gamma>>1$
it decreases rapidly with energy. Conversely,at very low energy, the annihilation rate is:

$R = NZ\, \pi\, r_e^2\, c\ (s^{-1})$, with $N=\rho\, N_A/A$

This rate corresponds to a lifetime in lead of about 10^{-10}s.
Positron annihilation plays a key role in some technical applications (Positron Emission Tomography)

<u>Interaction of electrons and positrons with nuclei: **Bremsstrahlung :**</u> Hard QED process
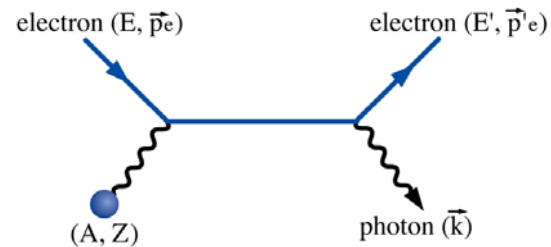
The spectrum of photons with energy k radiated by an electron traversing a thin slab of material (expressed as a function of y=k/E) has a characteristic "bremsstrahlung" spectrum(dominantly in 1/k) given by the differential cross-section.

$d\sigma/dk = 4\ \alpha\ Z(Z+1)r_e^2\ \ln(183Z^{-1/3})(4/3-4/3y+y^2)/k$

The average energy lost by bremsstrahlung is obtained by integrating over y,and is conveniently described by introducing the **radiation length X_0**

-dE/E = dx/X_0

   X_0 is the mean distance after which an electron has lost, by radiation, all but a fraction 1/e of its initial energy. X_0 also has a simple meaning in terms of photon conversion (see below).

$$1/X_0 = 4\,\alpha\,(N_A/A)\,[Z(Z+1)r_e^2\ln(183Z^{-1/3})]\,(cm^2\,g^{-1})$$

   The Z^2 term reflects the fact that the bremsstrahlung results from a coupling of the initial electron to the electromagnetic field of the nucleus somewhat screened by the electrons (log term), and augmented by a direct contribution from the electrons (Z^2 replaced by $Z(Z+1)$).

   For a compound or mixture: $1/X_0 = \Sigma\,w_j/X_j$
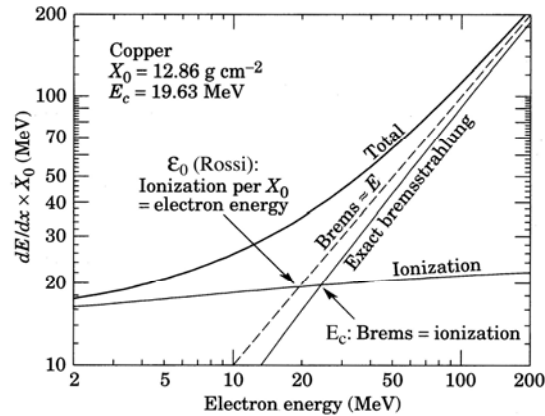
Average energy loss of electrons in Copper by ionization and bremsstrahlung.
   Two definitions of the critical energy (E_c and ε_0(Rossi)) are shown by arrows).
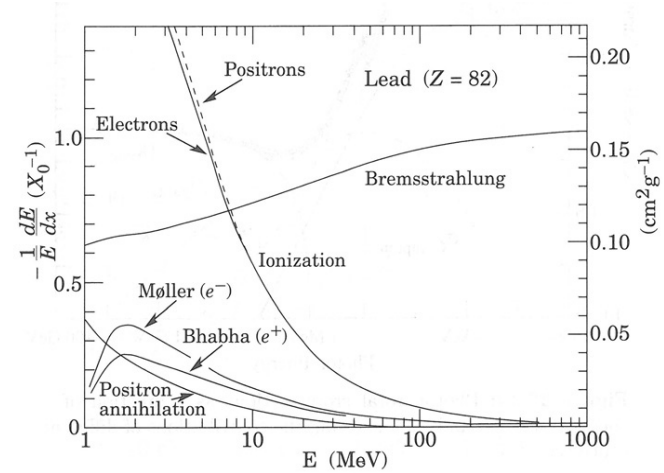
   Relative energy loss of electrons and positrons in lead
with the contributions of ionization, bremsstrahlung, Møller (e⁻) and Bhabha (e+) scattering and positron annihilation

The critical energy E_c for **electrons** (or positrons) in a given medium is defined as the energy at which energy loss by radiation in a thin slab equals the energy loss by ionisation. A slightly different definition ε_0, introduced by Rossi, results from considering the relative energy loss as fully independent of energy The critical energy ε_0 is well described in dense materials by:

ε_0 = 610 MeV/ (Z+1.24).

Electron critical energy for the chemical elements,
using Rossi's definition .
Solids and liquids (solid line) and gases (dashed line).
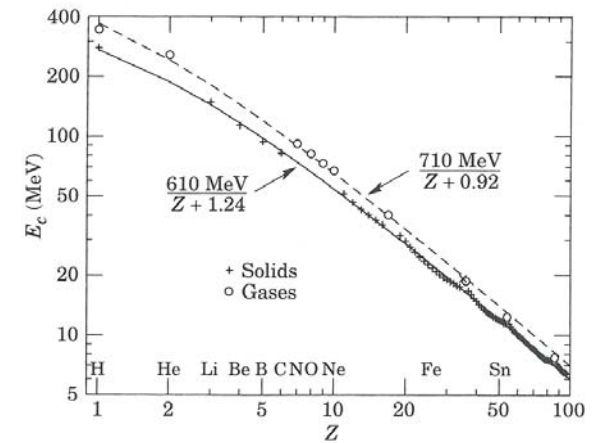
Interaction of photons with matter Again QED processes

- *Pair creation*

Dominant for photon energies above a few times $2\ m_e c^2$.
Dominant part (Z^2) is due to the nucleus.Electrons contribute proportionally to Z.
Pair creation cross-section:

$$d\sigma/dE = A/(X_0 N_A).(1-4/3x\ (1-x)),$$

where E is the fraction of the photon energy k taken by the electron of the pair, and x=E/k.

$$\sigma = 7/9\ A/(X_0 N_A) = 7/9\ 4\ \alpha\ Z(Z+1)r_e^2\ \ln(183Z^{-1/3})$$

After 9/7 of an X_0, probability that a high energy photon survives without having materialized into an electron-positron pair =1/e.
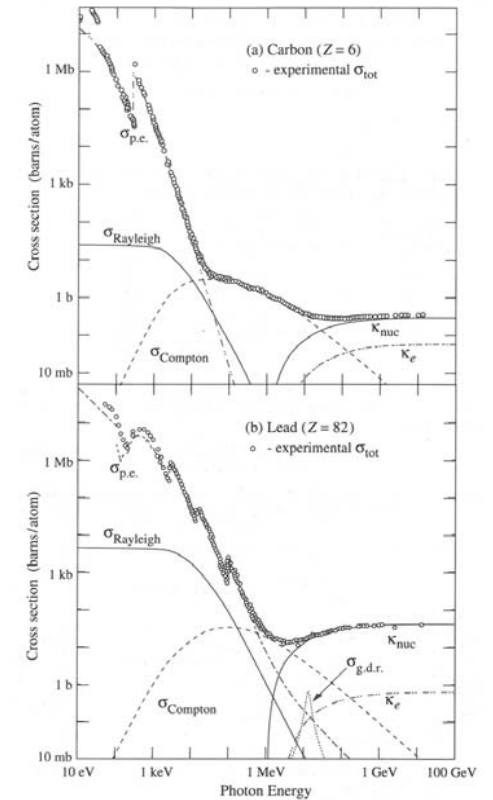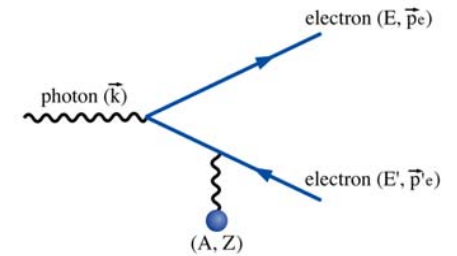Energy of the recoil nucleus is small($\sim m_e c^2$) $\rightarrow$electron and the positron are collinear.
If the reaction takes place with an electron, the momentum transfer can be higher $\rightarrow$ "triplets"

- *Compton effect*

QED cross-section for photon-electron scattering (Klein-Nishina [8]) for $k >> m_e c^2$ ($x=k/ m_e c^2$)

$$\sigma = \pi r_e^2\ (\log 2x +1/2)/x\quad (cm^2)$$

High Z (lead) Compton cross-section and pair production cross-section similar.
Lighter materials Compton cross-section is higher.

The differential Compton cross-section, introducing θ the diffusion angle between the initial and final photons, and η the angle between the perpendicular to the scattering plane and the polarization vector of the initial photon(in case it is linearly polarized) reads(ε being the ratio between the diffused and the incident photon energy $\varepsilon=1/(1+E_0/m_ec^2(1-\cos\theta))$:

$d\sigma/d\Omega = 0.5 \; r_e^2 \; (\varepsilon+1/\varepsilon-2 \; \sin^2\theta\cos^2\eta)$

At low energy the probability of backward scattering is sizeable.

- *Photo-electric effect.*

For low photon energies,atomic electrons are not free→cross-section
presents discontinuities whenever the photon energy crosses the electron binding energy.

- *VERY High energy effects (LPM)*

In the collinear approximation of bremsstrahlung, the longitudinal momentum difference
$q_{||}$ between the initial electron (energy E) and the sum of the final electron and photon (energy k) is equal to

$$q_{||} = m_e^2c^3k/2E(E-k)$$

This quantity can be extremely small, being for example 0.002 eV/c when a 25 GeV electron radiates a 10 MeV photon. Such a small longitudinal transfer of momentum implies a large formation length, L_f ($L_f \, q_{||} \geq h/2\pi$), about 100 μm in the above example.
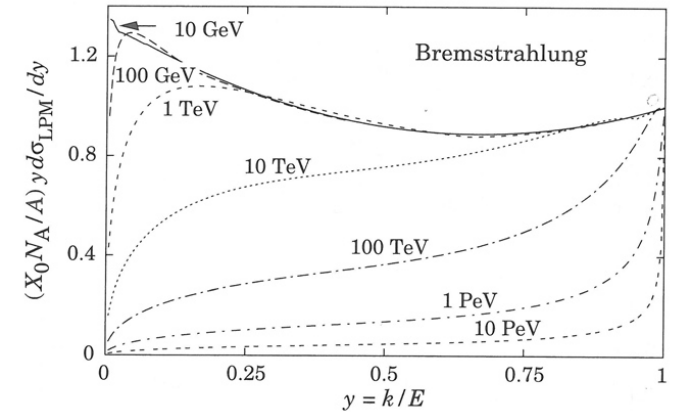
Normalized Bremsstrahlung cross-section
k dσ/dk in lead as a function of the fraction of momentum
taken by the radiated photon.

.

   Secondary interactions (like multiple scattering) taking place over this distance will
perturb the final state and will in general diminish the bremsstrahlung cross-section
and the pair production cross-section in case of photon interactions.
Coherent interaction of the produced photons with the medium (dielectric effect)
also affects, and reduces, the bremsstrahlung cross-section.

Hadronic interactions of photons

   $A(\gamma^*A \rightarrow B) = (e/2\gamma_\rho) \, m^2{}_\rho / (m^2{}_\rho - q^2) A(\rho A \rightarrow B)$ + equivalent terms for the ω and ϕ mesons

Ratio of hadron production to electron-positron pair production in the interaction of a 20 GeV
photon is about 1/200 for hydrogen and 1/2500 for lead

1.2 Electromagnetic showers

   Shower results from cascading effects: electron makes a brem which in turn converts in a
pair,…..

- *Analytical description*

   $-c(E_0,E,t)$ the average number of electrons plus positrons with energy between
E and E+dE at depth t   [integral distribution $C(E_0,E,t) = \int_E^\infty c(E_0,E',t) \, dE'$]
   $-n(E_0,E,t)$ and $N(E_0,E,t)$, the corresponding functions for photons.

   From Bremsstrahlung, Compton, dE/dx, pair production →"evolution equations"
correlating $C(E_0,E,t)$ and $N(E_0,E,t)$.,which can then be calculated(Rossi)
The total track length TTL = $\int_0^\infty C(E_0,0,t) \, dt$ represents, once multiplied by ε_0 ,
the energy transferred to the calorimeter medium by dE/dx, the source of the calorimeter signal.
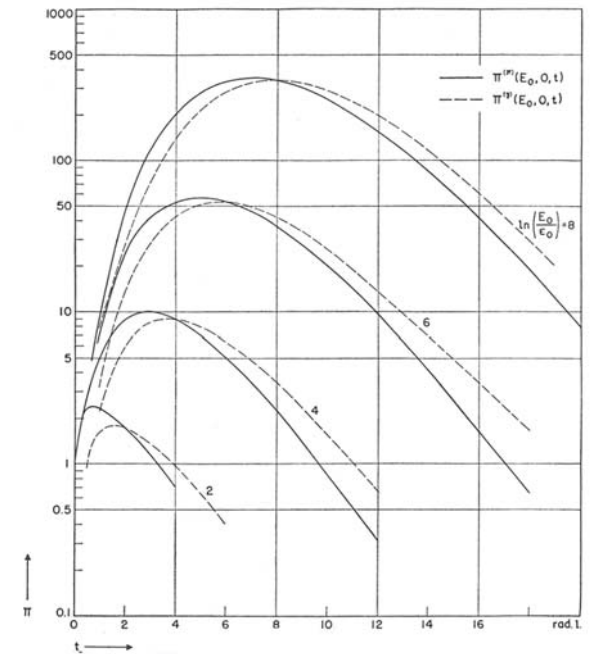
Electrons in an electron
induced(plain line) or photon
induced shower.

- *Monte Carlo simulations*

Monte-Carlo (MC) simulations reproduce step by step, in a randomized manner, the physical effects governing the shower formation. For several decades the standard simulation package has been EGS4 . This code has been transported/rewritten in the Geant 4 framework

EGS4 simulation of a 30 GeV electron induced cascade in iron.
- histogram : fractional energy deposition per radiation length
- curve is a gamma function fit to the distribution
- full (open) points represent the number of electrons (photons) with energy greater than 1.5 MeV crossing planes at $X_0/2$ internals

Remark: energy deposition and number of electrons are very similar,but not Identical.One reason is that toward shower end ,electrons scatter which increase their path and thus their energy loss/0.5 X0
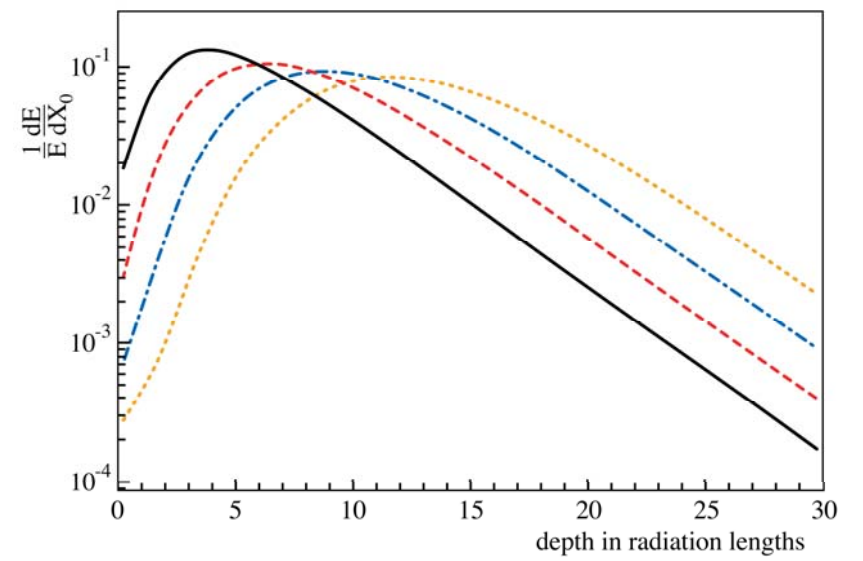
$F(E,t)= E_0\, b\, (bt)^{a-1}\, e^{-bt}/\Gamma(a)$ Longo and Sestili:

with $t_{max}=(a-1)/b$, well fitted by $t_{max}= \ln(y) + C_i$, ($C_i= 0.5$ for photons,-0.5 for electrons).
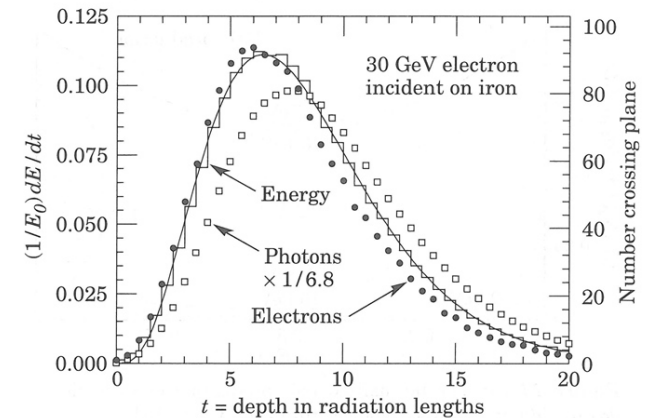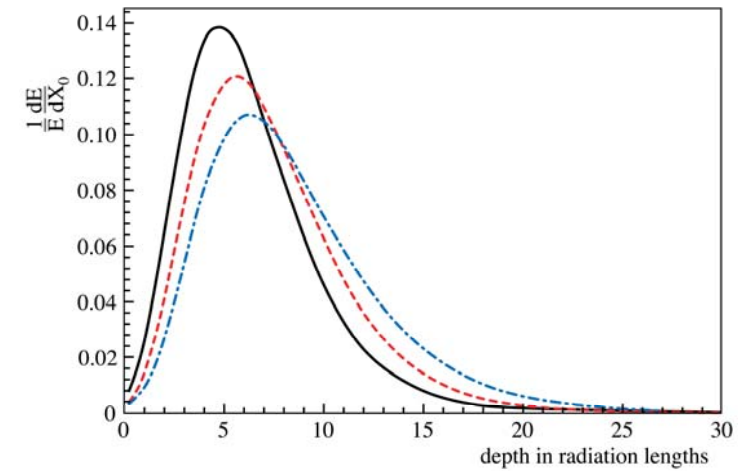
Fractional energy deposition in lead, per longitudinal slice of $1X_0$, for electron induced showers of 1 GeV (full line), 10 GeV (dashed), 100 GeV (dash-dot) and 1 TeV (dotted) (Geant 4).

Every 10 GeV the shower moves deeper by ~2 X0

Fractional energy deposition per longitudinal slice of $1X_0$ for 10 GeV electrons in aluminium (full line), copper (dashed) and lead (

- *Lateral shower development*

Bremsstrahlung on electrons and Compton scattering involve some momentum transfer.

Example, in the Compton interaction of a 2 MeV (0.5 MeV) photon, 6% (16%) of the scattered photons are emitted with an angle larger than 90° with respect to the initial photon direction(z).

The other important effect is due to the multiple scattering of electrons and positrons.

$$\theta_{x,y} = \frac{E_s}{\sqrt{2}} \frac{1}{p\beta c} \sqrt{l / X_0}$$

$$\delta_{x,y} = \frac{\theta_{x,y} l}{\sqrt{3}}$$

$$E_s = m_e c^2 \sqrt{(4\pi/\alpha)} = 21.2 \text{ MeV}$$

To quantify the transverse shower spread : Moliere radius $\rho_M = E_s X_0/E_c$,

From MC : about 87% (96%) of the energy in a shower is contained in a cylinder of radius 1 (2) ρ_M.

$\rho_M \sim$ independent from the nuclear species; governed by the material density

Fractional energy deposition in cylindrical layers of thickness 0.1 ρ_M, coaxial

with the incident particle direction, for 100 GeV electron induced

showers developing in aluminium (full line), copper (dashed line) and lead

(dash-dotted) (Geant4).
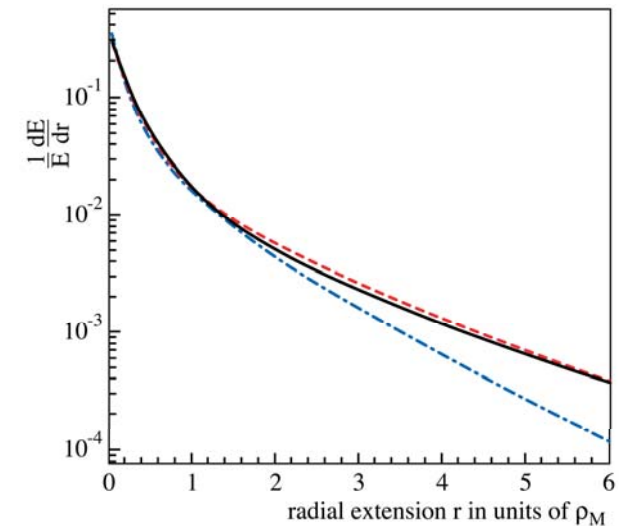
90% containment radius R$_{90\%}$(full line), in Molière radius ρ_M as a

function of shower depth, for 100 GeV electron showers developing

in lead. For comparison the longitudinal profile is also shown(Geant4)
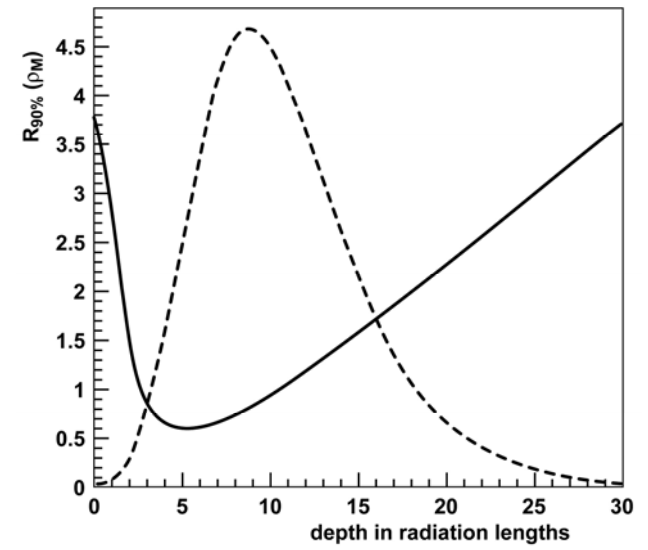
Properties of calorimeter materials.

Material	Z	Density $[g\,cm^{-3}]$	E_c [MeV]	X_0 [mm]	ρ_M [mm]	λ_{int} [mm]	$(dE/dx)_{mip}$ $[MeV\,cm^{-1}]$
C	6	2.27	83	188	48	381	3.95
Al	13	2.70	43	89	44	390	4.36
Fe	26	7.87	22	17.6	16.9	168	11.4
Cu	29	8.96	20	14.3	15.2	151	12.6
Sn	50	7.31	12	12.1	21.6	223	9.24
W	74	19.3	8.0	3.5	9.3	96	22.1
Pb	82	11.3	7.4	5.6	16.0	170	12.7
^{238}U	92	18.95	6.8	3.2	10.0	105	20.5
Concrete	-	2.5	55	107	41	400	4.28
Glass	-	2.23	51	127	53	438	3.78
Marble	-	2.93	56	96	36	362	4.77
Si	14	2.33	41	93.6	48	455	3.88
Ge	32	5.32	17	23	29	264	7.29
Ar (liquid)	18	1.40	37	140	80	837	2.13
Kr (liquid)	36	2.41	18	47	55	607	3.23
Polystyrene	-	1.032	94	424	96	795	2.00
Plexiglas	-	1.18	86	344	85	708	2.28
Quartz	-	2.32	51	117	49	428	3.94
Lead-glass	-	4.06	15	25.1	35	330	5.45
Air 20°, 1 atm	-	0.0012	87	304 m	74 m	747 m	0.0022
Water	-	1.00	83	361	92	849	1.99

2 Homogeneous and sampling calorimeters

2.1 definitions

Homogeneous calorimeter = built only from the sensitive medium.
Sampling calorimeter = stack of passive and active layers :
     resolution limited by 'sampling fluctuations'.

Homogeneous Calorimeters for low energies
Germanium (Li-doped) crystal exposed to a γ source of ^{108m}Ag and ^{110m}Ag.
In a semi-conductor(Germanium) it takes about 2.9 eV to create an electron-hole pair
$\rightarrow N=E/\varepsilon$ .Assuming statistical independance $\sigma=\sqrt{N}/N$ for a 1 MeV line one expects
a relative width of $\sim 2 \times 10^{-3}$
Experimentally the line is narrower : Reason for this kind of phenomena
first understood by Fano   : Correlation by $\Sigma\varepsilon$ exactly=E
In practice ε has some dispersion,call it σ $\rightarrow$the actual resolution should be $\sigma/(\varepsilon\sqrt{N}p)$,
 smaller than $1/\sqrt{N}p$ by a factor $\sqrt{F}$, where $F=(\sigma/\varepsilon)^2$ is the Fano factor.
Monte-Carlo simulations reproduce the phenomenon and give $F\sim 0.1$
for semi-conductor devices, in reasonable agreement with measurements .
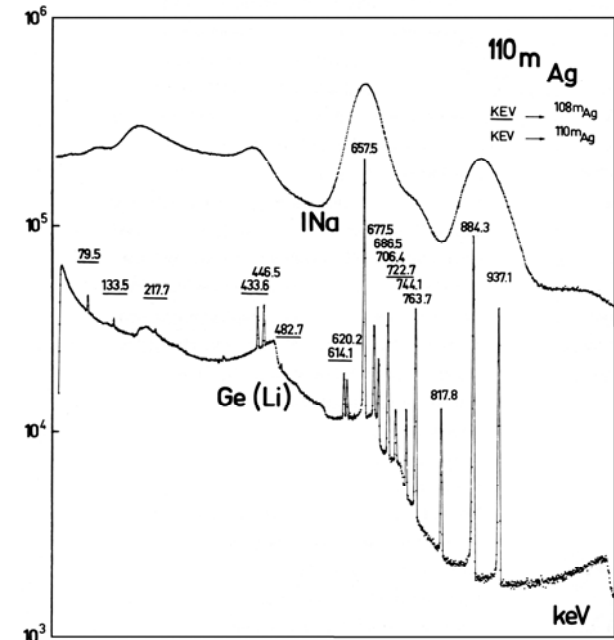
Pulse height spectra recorded using a sodium
iodide scintillator and a Ge (Li) detector.
The source = gamma from the decay of ^{108m}Ag
and ^{110m}Ag.

When two or more energy loss mechanisms compete, e.g. ionisation and scintillation, the total energy constrain remains, but with a binomial sharing between the two mechanisms.
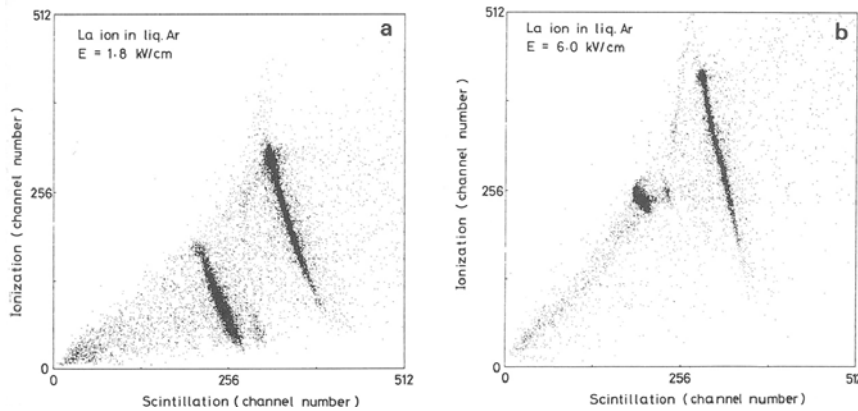
Correlation between scintillation signals and charge signals for an electric field of (a)1.8 kV/cm and (b) 6.0 kV/cm in the grid-cathode space (only the lower energy band corresponds to charge deposits confined to the grid-cathode space)

Saturation effects (Birk's law)

(affects bot homogeneous and sampling calorimeters)

For scintillators,some saturation is observed for high density(low velocity fragments) deposits

$$dL/dx = L_0 \cdot dE/dx/(1.+k_B \, dE/dx) \qquad (L_0 : \text{ luminescence at low specific ionisation density})$$

-Plastic scintillators : $k_B \sim 0.01$ g.cm^{-2}MeV^{-1}, is associated to suppression ("quenching") of the light emission by the high density of ionized and excited molecules. Deviations to Birks law have been observed for high Z ions .

-In liquid ionisation detectors the effect is associated with electron-ion recombination. It depends upon the electric field, in magnitude and direction with respect to the ionizing track. A typical value in liquid argon is $k_B \sim 0.04$ g.cm^{-2}MeV^{-1} for an electric field in a direction perpendicular to the track of 1kV/cm, with k_B being inversely proportional to E for E< 1 kV/cm .

Saturation effects are not relevant for electron or photon induced showers (at least below few TeVs) because the track density remains comparatively low

Saturation effects do affect hadronic showers because of slow, highly ionizing fragments from nuclear break-up, and slow proton recoils.

The-in general excellent-energy resolution of homogeneous calorimeters used for electromagnetic showers is affected by several effects.

-Existence of a threshold energy E_{th} below which an electron of the shower does not produce a signal: example =Cherenkov

Other effects include:

-longitudinal and transverse shower containment

-efficiency of light collection

-photo-electron statistics

-electron carrier attachment (impurities)

-space charge effects ,…

.

2.2 Sampling calorimeters and sampling fluctuations

The thickness t of the passive layers (in units of X_0) determines the sampling frequency, i.e. the number of times a high energy electron or photon shower is 'sampled '.

Intuitively, the thinner the passive layer (i.e. the higher the sampling frequency), the better. The thickness u of the active layer (in units of X_0) is characterized by the **sampling fraction** f_S [defined by quantities for minimum ionizing particles]

$$f_S = u.dE/dx_{active}/[u.dE/dx_{active} + t.dE/dx_{passive}]$$ (u,t in gcm^{-2}, dE/dx in MeV/gcm^{-2}).

An approximate expression for the fluctuations in electromagnetic calorimeters can be expressed using the total track length (TTL)

The signal is approximated by the number N_x of e^+ or e^- traversing the active signal planes, spaced by a distance (t+u).

This number N_x of crossings is

$$N_x = TTL / (t+u) = E / \varepsilon_0 (t+u) = E / \Delta E,$$

ΔE being the energy loss in a unit cell of thickness (t+u). Assuming statistical independence of the crossings, the fluctuations in N_x represent the 'sampling fluctuations' $\sigma(E)_{samp}$,

$$\sigma(E)_{samp}/E = \sigma(N_x)/N_x = 1/\sqrt{N_x} = [\Delta E(GeV)/E(GeV)]^{\frac{1}{2}} = a /\sqrt{E} .$$

a is often called the "sampling term" of the energy resolution .

For example, for a lead/scintillator calorimeter with 1.4 mm lead plates, interleaved with 2 mm scintillator planes, $\Delta E = 2.2$ MeV, $\rightarrow \sim 5\%$ for 1 GeV electromagnetic showers. The experimental value is closer to 7 to 8% ,because of:

- threshold effects in signal emission
- angular spread of electrons around the shower axis
- a large fraction of the shower particles are produced as e^+e^- pairs, reducing the number of statistically independence crossings N_x .

The sampling fraction f_S may also have practical consequences considering the actual signal produced by the calorimeter which is directly proportional to $\Sigma u dE/dx/E$ (E is the energy of the incident electron or photon). If f_S is too small, the signal is small and may be affected by electronics noise and possibly other technical limitations due to the chosen readout technique (see below).

The dominant part of the calorimeter signal is not produced by minimum ionizing particles, but rather by the low-energy electrons and positrons crossing the signal planes. Defining the fractional response f_R of a given layer "i" as the ratio of energies lost in the active and of the sum of active plus passive layers one has

$$f_R^{\ i} = E^i_{active} / (E^i_{active} + E^i_{passive})$$

with the constraint that $\Sigma^i (E^i_{active} + E^i_{passive}) = E_0$.

Data have shown that f_R (taking all layers together) is significantly smaller than f_S.

f$_R$/ f$_S$, usually called 'e/mip' can be as low as 0.6 when Z of the passive material (lead) is much larger than Z of the active one
  This effect, well reproduced by Monte-Carlo simulations is due to
     -the transition effect between the passive and active material
     -the fact that a significant fraction of electrons produced in the high Z passive material by pair production or Compton scattering do not have enough energy to exit this layer and are thus not sampled.
   Taking into account a constant contribution from electronics noise b, and a minimum asymptotic value of the relative energy resolution c (constant term, due for example to inhomogeneities in materials, imperfection of calibrations,…) the energy resolution of a sampling calorimeter is in general written as

$$\Delta E/E = a / \sqrt{E} \oplus b/E \oplus c.$$

Experimentally it has been observed that the same relation holds also for homogeneous calorimeters, in general with smaller "sampling terms" a, although their origin is not coming from sampling fluctuations, but from other limitations

2.3 Physics of the hadronic cascade

The energy degradation of high-energy hadrons proceeds through an increasing number of (mostly) strong interactions with the calorimeter material.
 Hadronic and nuclear processes produces a multitude of effects that make hadronic calorimeters more complicated instruments to optimize and results in a significantly worse intrinsic resolution .
The hadronic interaction produces two classes of secondary processes:
   - energetic secondary hadrons with momenta typically a fair fraction of the primary hadron momentum, i.e. at the GeV scale.
   -a significant part of the primary energy is diverted to nuclear processes such as excitation, nucleon evaporation, spallation, etc., resulting in particles with characteristic nuclear energies at the MeV scale.
This is reflected by the spectra of energies of the major shower components (weighted by their track length in the shower) averaged over many cascades, induced by 100 GeV protons in lead.

These spectra are dominated by electrons, positrons, photons, and neutrons at low energy. The structure in the photon spectrum at approximately 8 MeV reflects an (n, γ) reaction and is a fingerprint of nuclear physics; the line at 511 keV results from e+e− annihilation photons. These low-energy spectra encapsulate all the information relevant to the hadronic energy measurement.
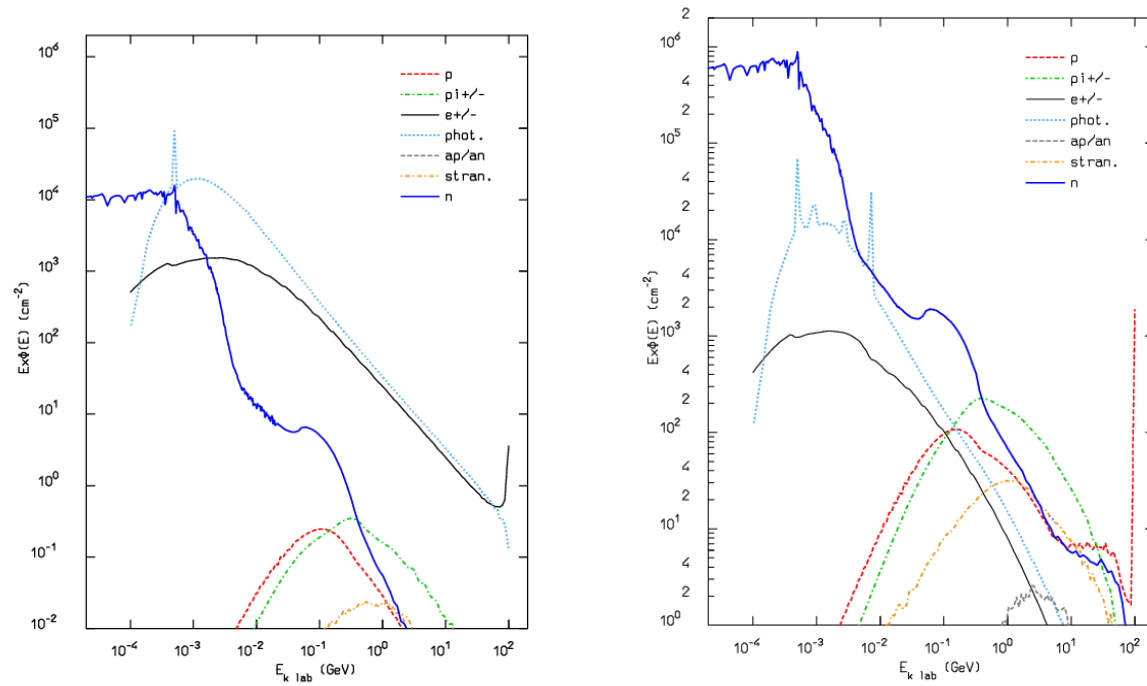
Fluences in Electromagnetic(left) and hadronic(right) showers from FLUKA

<u>The energetic component</u> contains protons, neutrons, charged pions and photons from neutral pion decays.

Charge independence of hadronic interactions → one third of the pions produced will be π^0's, $f_{\pi 0} \approx 1/3$. These neutral pions will decay to two photons, and will induce an electromagnetic cascade.

This physics process acts like a 'one-way diode', transferring energy from the hadronic part to the electromagnetic component, which will not contribute further to hadronic processes.

As the number of energetic hadronic interactions increases with increasing incident energy, so will the fraction of the electromagnetic cascade. This simple picture of the hadronic showering process leads to a power law dependence of the two components naively, the electromagnetic component $F_{em} = 1-(1- f_{\pi 0})^n$, n denoting the number of shower generations induced by a particle with energy E.

. As the energy of the incident hadron increases, Fem increases.

Extrapolating this law to the highest particles energies detected calorimetrically, $E \leq 10^{20}$ eV more than 98 % of the hadronic energy would be transformed into electromagnetic energy!

<u>The low-energy nuclear part</u> of the hadronic cascade has very different properties,
but carries the dominant part of the energy in the hadronic sector.
In the energetic hadron-nucleus collisions, nucleons will be struck themselves
initiating an 'intra-nuclear' cascade.
In the subsequent steps, the intermediate nucleus will de-excite, in general
through a spallation reaction, evaporating a considerable number of nucleons,
accompanied by few MeV γ-emission. .
 The number of these low-energy neutrons is large: ~ 20 neutron/GeV in lead.
 The fraction of the total associated binding energy depends on the incident energy
and may be as high as ~ 20-40%. These neutrons will ultimately be captured

by the target nuclei, resulting in delayed nuclear photon emission (at the ~ μs timescale).
 The energy lost to binding energy is therefore, in general, not detected ('invisible')
in practical calorimeters.
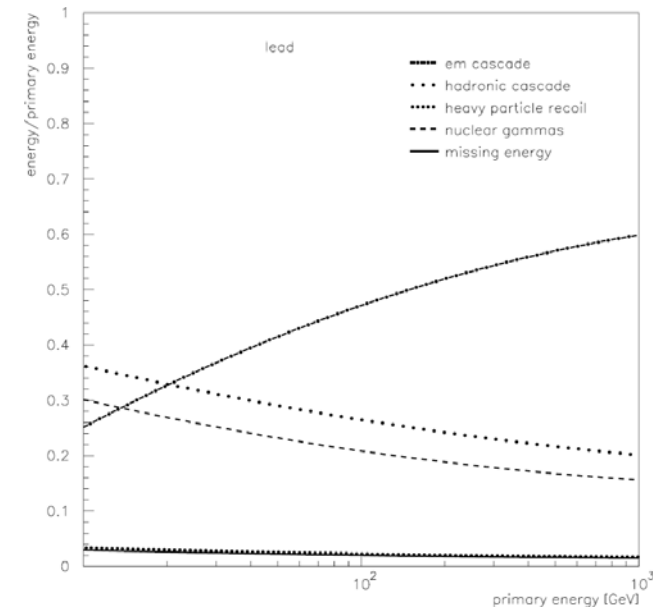
. The road to high-performance hadronic calorimetry has been opened by understanding how to compensate for these invisible energy fluctuations

2.4 Hadronic shower profile.

Total cross section for hadrons weakly energy-dependent in the range 50 to 300 GeV.
For protons the total pp cross section σ_{tot} is approximately 39 mb.
For pion-proton collisions $\sigma_{tot}(\pi p) \sim 2/3\ \sigma_{tot}(pp)$ expected i.e. 26 mb, compared to the measured value of ≈ 23 mb.
For hadronic calorimetry the inelastic cross sections, $\sigma_{inel}(pA)$ or $\sigma_{inel}(\pi A)$, determine the corresponding interaction length, $\lambda_{int} = A / N_A\sigma_{inel}(hadron,A)$.
On geometrical grounds $\sigma_{inel}(hadron, A)$ is expected to scale as $A^{2/3}\sigma_{inel}(hadron, p)$, close to the measured approximate scaling $A^{0.71}\sigma_{inel}(hadron, p)$.

Therefore $\lambda_{int} \approx A^{0.29}/[N_A\sigma_{inel}(hadron,p)]$ [gcm^{-2}].

In analogy to the parameterization of electromagnetic showers the longitudinal profile of hadronic showers can be parametrized in the form
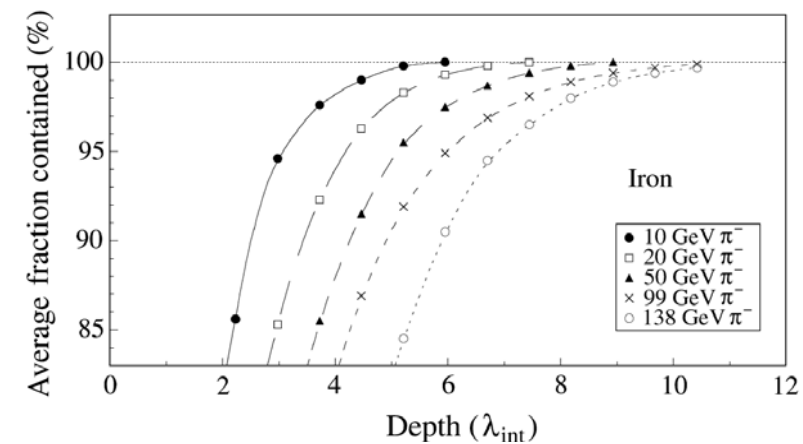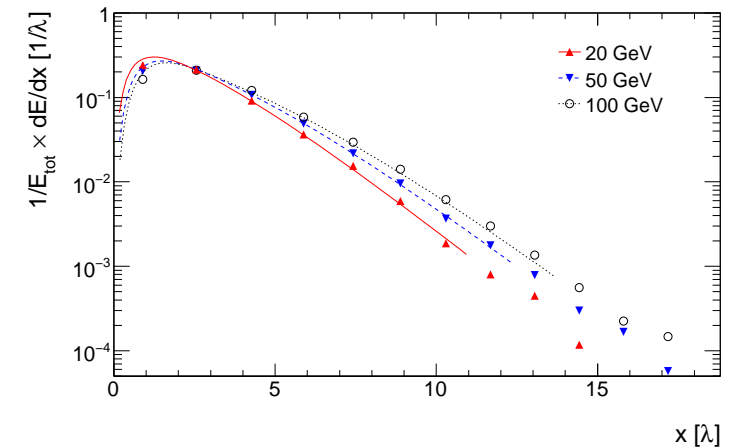
$$dE/dx = c\{w(x/X_0)^{\alpha-1} \exp(-bx/X_0) + (1-w)(x/\lambda)^{\alpha-1}\exp(-dx/\lambda)\}.$$

2.5 Energy resolution of hadron calorimeters

- η_e scale for observing a signal E^e_{vis} (visible energy) from an electromagnetic shower, i.e., $E^e_{vis} = \eta_e E(em)$
- η_h be the corresponding scale for purely hadronic energy

Decomposing a hadron-induced shower into the em fraction F_{EM} and a purely hadronic part F_h the measured energy E^π_{vis} for a pion-induced shower is

$$E^\pi_{vis} = \eta_e F_{EM}E + \eta_h F_h E = \eta_e (F_{EM} + \eta_h/\eta_e F_h)E \qquad \text{(E initial pion energy)}$$

The ratio of observable signals induced by electromagnetic and hadronic showers, usually denoted 'e/π,' is therefore

$$E^\pi_{vis}/ E^e_{vis} = (e/\pi)^{-1} = 1 - (1 - \eta_h/\eta_e)F_h .$$

In general $\eta_h i < \eta_e \rightarrow$ the average response of a hadron calorimeter as a function of energy will not be linear because F_h decreases with incident energy. More subtly, for $\eta_h \neq \eta_e$, event-by-event fluctuations in the F_h and F_{EM} components produce event-by-event signal fluctuations and impact the energy resolution of such instruments.

The relative response 'e/π' is the most important yardstick for gauging the performance of a hadronic calorimeter.
:

- – fluctuations in F_{EM} are a major contribution to the energy resolution;
- – the average value (F_{EM}) increases with energy: such calorimeters have a non-linear energy response to hadrons ;

– these fluctuations are non-Gaussian and therefore the energy resolution scales weaker than $1/\sqrt{E}$.

Suggests to 'tune' the e/π response of a calorimeter in the quest for achieving e/π = 1

Conceptual response of calorimeters to electrons and hadrons.
The curves are for a 'typical' sampling calorimeter
with electromagnetic resolution of $\sigma/E = 0.1/\sqrt{E(GeV)}$, with
hadronic resolution of $\sigma/E = 0.5/\sqrt{E(GeV)}$ and e/π = 1.4.
The hadron-induced cascade fluctuates between almost
completely electromagnetic and almost completely hadronic
energy deposit, broadening the response and producing
non-Gaussian tails.

Signal (in energy units) obtained for a 10 GeV energy deposit
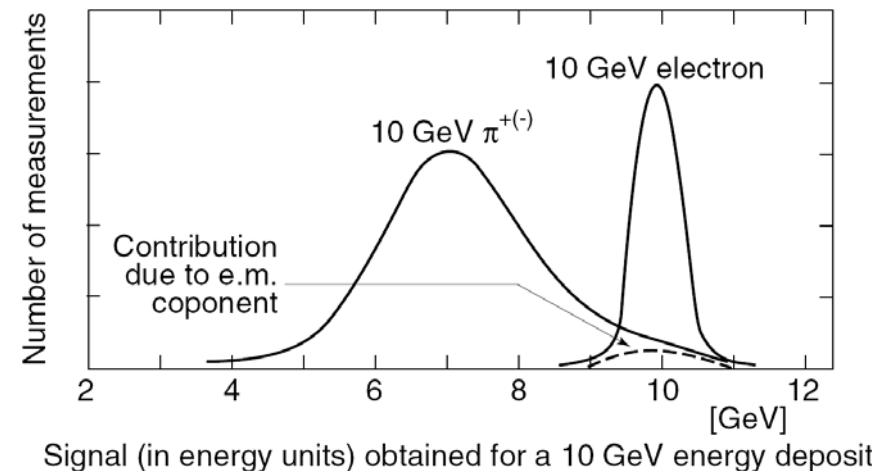
For this purpose the role of what happens to neutrons is essential:Walk of neutrons with energies $E_n < 1$–2 MeV is dominated by elastic scattering; cross-sections are large (~ barns) and mean free paths short (a few centimeters); the energy loss is ~1/A (target) and hence small. Once thermalized, a neutron will be captured, giving rise to γ-emission.

This abundance of neutrons gives a privileged role to hydrogen which may be present in the readout material. In a n-p scatter on average half of the neutron kinetic energy is transferred. The recoil proton, if produced in the active material, contributes directly to the calorimeter signal, i.e., is not sampled like a mip (a 1 MeV proton has a range of ~20 μm in scintillator).
. Changing the sampling fraction allows to alter, to 'tune' e/π.

This approach works well for high-Z absorbers with a relatively large fission cross section, accompanied by multiple neutron emission. Optimised ratios tend to imply for practical scintillator thicknesses rather thick absorbers with concomitant significant sampling fluctuations and reduced signals.

One observes a significant reduction in the fluctuations and an intrinsic hadronic energy resolution of $\sigma/E \approx 0.2/\sqrt{E(GeV)}$ for instruments with $e/\pi \approx 1$.
Detectors achieving compensation for the loss of non-detectable ('invisible') energy, i.e., $e/\pi = 1$, are called 'compensated' calorimeters.

Contributions to and total energy resolution of 10 and 100 GeV hadrons in scintillator calorimeters as a function of thickness of a) uranium plates and b) lead plates. The scintillator thickness is 2.5 mm in both cases. The dots in the curves are measured resolution values of actual calorimeters
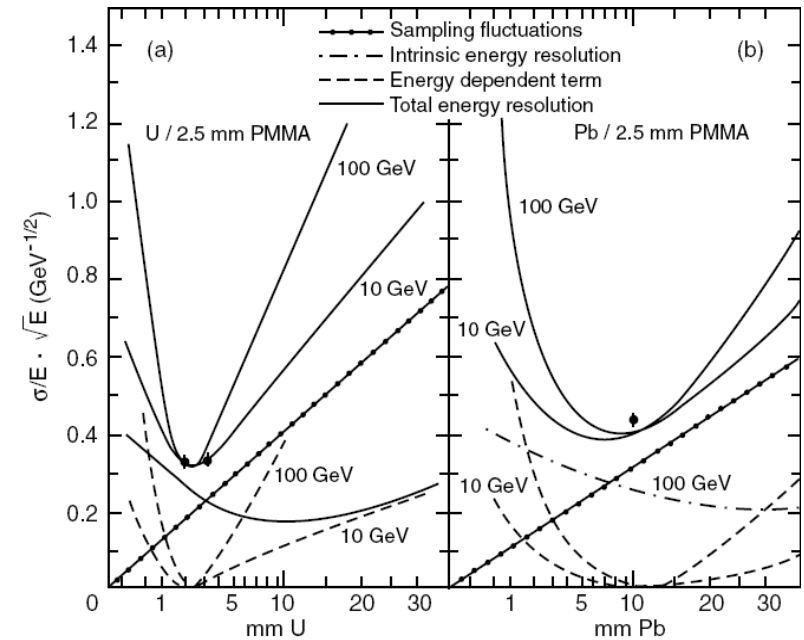
Sampling fluctuations in hadronic calorimeters

-For electromagnetic calorimeters a simple explanation and an empirical parameterization holds:

$\sigma_{samp}(em)/E = c(em) \cdot (\Delta E(MeV)/E(GeV))^{1/2}$, where ΔE is the energy lost in one sampling cell and c (em) ≈ 0.05 to 0.06 for typical absorber and readout combination.

- Similar arguments apply for the hadronic cascade; empirically, one has observed that

$\sigma_{samp}(h)/E = c(h) \cdot (\Delta E(MeV)/E(GeV))^{1/2}$ with c(h) ≈ 0.10.

The foundations of modern, optimized hadron calorimetry can be summarized as follows:
- the key performance parameter is e/π = 1, which guarantees linearity, $E^{-1/2}$ scaling of the energy resolution, and best resolution;
- by proper choice of type and thickness of active and passive materials the response can be tuned to obtain (or approach) e/$\pi \sim 1$
- the intrinsic resolution in practical hadron calorimeters can be as good as (σ/E) $\cdot \sqrt{E} < \sim 0.2$;
- sampling fluctuations contribute at the level of $\sigma/E \approx 0.10 (\Delta E(MeV)/E(GeV))^{1/2}$.

2.6 Muons in a dense material

At low energy,muons encounter only energy loss by dE/dx
(no nuclear interaction,no bremsstrahlung)

However for muon energies above ~100 GeV, bremsstrahlung,
pair production and deep inelastic scattering start to contribute,
generating tails in the energy distribution ('catastrophic energy loss').
  Very roughly speaking a muon behaves as an electron with a critical
energy scaled as $\approx (m_\mu / m_c)^2$.

However, unlike for electrons or positrons, pair production (trident)
is larger than bremsstrahlung.
  Similar effects are also present for charged pions, of only slightly
larger mass, but are obscured by the strong interaction of pions
which generate a hadronic cascade.

Contributions to the energy loss of muons in iron,
as a function of the muon incident energy.
The total energy loss in gas hydrogen and uranium is also shown.
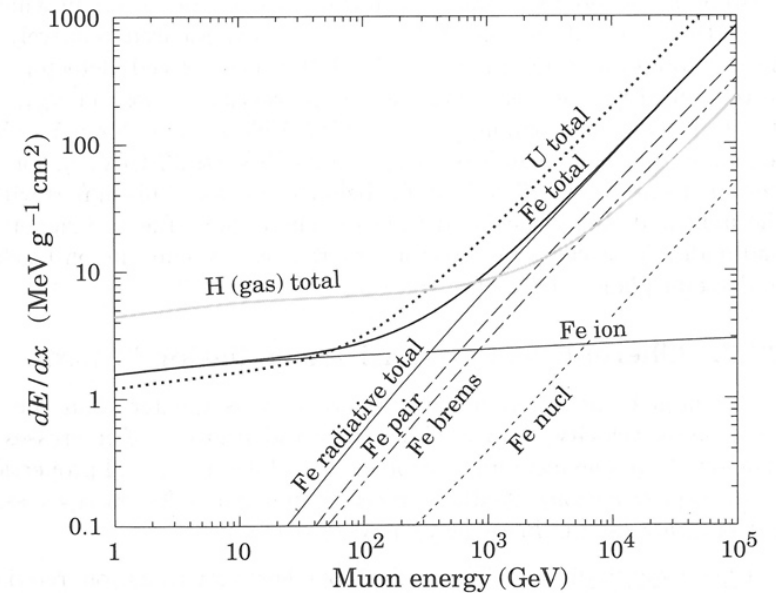
Because they deposit their energy locally, and with a well defined average,muons are heavily used to "scan through" calorimeters and get information on alignment,dead cells,…

2.7 Monte Carlo Simulation of hadronic calorimeter response

Modern calorimetry would not have been possible without extensive shower simulations.
Done first to understand electromagnetic calorimeters. EGS4, has become the standard (and is now integrated/rewritten in Geant 4)
For hadronic simulations it were the codes developed by the Oak Ridge group with their extensive modelling of nuclear physics, neutron transport, spallation and fission, which are indissociable from the development of modern hadron calorimetry .

GEANT 4   provide the user with choices of physics interaction models to adapt to a given experimental situation.
At high energies (~15 GeV to ~100 TeV) models describing the hadron physics are used, such as the 'Quark Gluon String' or Dual Parton Models
In the intermediate energy range (<10 GeV) Bertini-style cascade models are employed to describe the intra-nuclear cascade phenomena. These models use measured cross-sections and angular distributions. Precision calorimetry is quite sensitive to the quality of the cascade description.
For the very low energy (< 20 MeV) domain neutron transport codes have been developed, using experimental cross-sections.
The different energy regimes covered by these models are connected with parametric descriptions, in which cross-sections are parameterized and extrapolated over the full range of hadronic shower energies.

Applications: illustrative examples
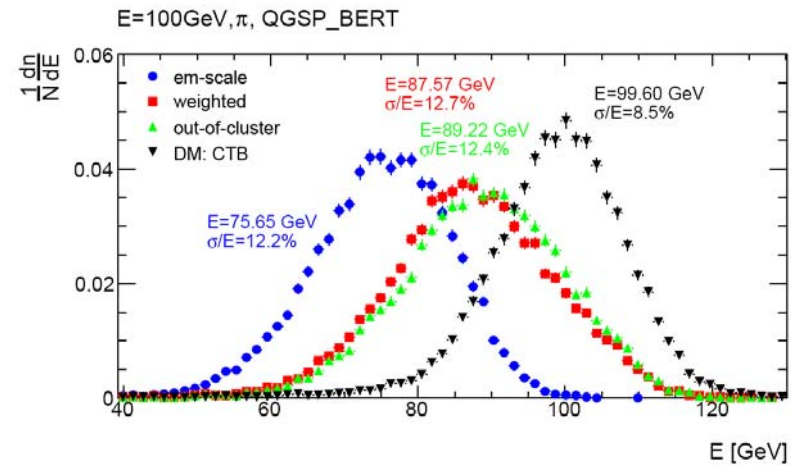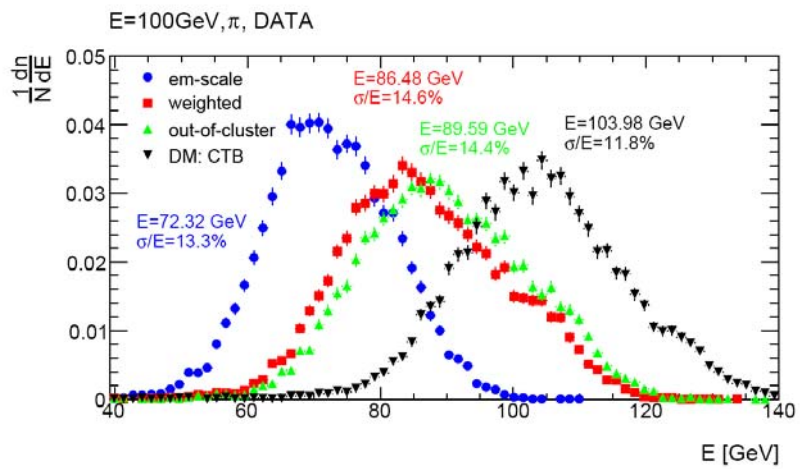
Reconstruction steps, to arrive at the reconstructed energy (100 GeV pions) in the MC (top panel) and for measurements (left panel) [58].

.

3 Readout methods in calorimeters

3.1 Scintillation light collection and conversion

 Scintillator materials used in calorimetry are inorganic crystals, organic compounds and noble liquids.

-Crystals: Dense inorganic crystals represent one of the best techniques for homogeneous electromagnetic calorimetry .

-These crystals are insulators with a normally empty conduction band. When energy is deposited in the crystal, an electron can jump into the conduction band and cascade to the valence band by intermediate acceptor levels, part of the energy being emitted as light. The emitted light needs to be in the wavelength range where good photodetectors are available, and the crystal must be transparent to this wavelength range. The lifetime of the light emission depends on the concentration of acceptor levels, and temperature.

-The existence of alternative des-excitation paths like by phonon emission shortens the lifetime but diminishes the light yield.

	NAI(Tl)	CsI(Tl)	CsI	BaF$_2$	CeF$_3$	BGO	PbWO$_4$
Density [g cm^{-3}]	3.67	4.51	4.51	4.89	6.16	7.13	8.30
Radiation length [cm]	2.59	1.85	1.85	2.06	1.68	1.12	0.89
Molière radius [cm]	4.8	3.5	3.5	3.4	2.6	2.3	2.0
Interaction length [cm]	41.4	37.0	37.0	29.9	26.2	21.8	18.0
$(dE/dx)_{mip}$ [MeV cm^{-1}]	4.79	5.61	5.61	6.37	8.0	8.92	9.4
Refractive index [at λ_{peak}]	1.85	1.79	1.95	1.50	1.62	2.15	2.2
Hygroscopicity	Yes	Slight	Slight	No	No	No	No
Emission spectrum, λ_{peak}							
Slow component [nm]	410	560	420	300	340	480	510
Fast component [nm]			310	220	300		510
Light yield relative to NaI							
Slow component	100	45	5.6	21	6.6	9	0.3
Fast component			2.3	2.7	2.0		0.4
Decay time [ns]							
Slow component	230	1300	35	630	30	300	50
Fast component			6	0.9	9		10

Crystals are usually shaped as bars, of ~25 X_0 length and ~1x1 ρ_M transverse size.

The light detector (photomultiplier, photodiode...) is optically coupled to the back face of the crystal.

The overall light yield, including the area and quantum efficiency of the transducer influences the achievable energy resolution.

A light yield of 1 photoelectron per MeV implies that the energy resolution cannot be better than $\sigma(E)/E = 3\%/\sqrt{E}$ (GeV) [Fano reasonning does not apply here in general]

The number of emitted photons per MeV is in general much larger, being for example 4.10^4 in NaI doped with Thallium, one of the best scintillating crystal in terms of light yield.

$PbWO_4$ produces ~150 times less light than NaI, but is far superior in other aspects (density, radiation resistance).

One of the main drawbacks is that crystals cannot be split in smaller readout cells for better particle identification/position measurement,..
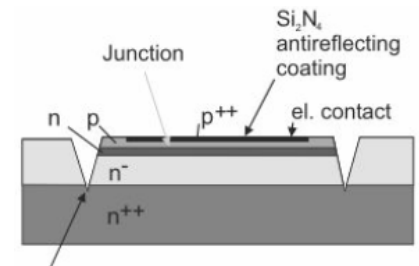
APD: amplification takes place in the thin p-n transition

Photodiodes and Avalanche photodiodes offer good quantum efficiency, absence of magnetic field sensitivity, moderate cost, small volume and –for APDs -a significant gain.

-The amplification is accompanied by an "excess noise factor", of typically a factor 2 for a gain of ~50.

-The light to electron conversion followed by electron multiplication takes place in a reduced thickness (<40 μm) which lowers the sensitivity of APDs to minimum ionizing particles traversing the crystal, as compared to simpler photodiodes.

Crystal calorimeters are the choice technology for precision electromagnetic calorimetry at medium energy machines like B-factories. The L3 experiment at LEP used BGO with success, but was not able to reach, over the complete system, the energy resolution that the technique in principle provides.

CMS (and ALICE for their PHOS modules) at the LHC use $PbWO_4$.

Noble liquids are also good, fast scintillators (comparable to NaI in light yield).The mechanism of light emission is of course Different and involves intermediate diatomic states.

| Property ↓ Liquid →	LAr	LKr	LXe
Z	18	36	54
Boiling point [K]	87.3	119.8	165.0
Density in liquid phase [g cm^{-3}]	1.40	2.41	2.95
Radiation length [cm]	14.0	4.7	2.40
Molière radius [cm]	8.0	5.5	4.2
Nuclear interaction length for protons [cm]	84	61	57
Ionization properties			
Energy needed per electron-ion pair [eV]	24	17	15
Drift speed (mm/µs at 10 kV/cm)	5	3.8	2.6
Scintillation properties			
Emission spectrum, λ_{peak} [nm]	128	147	174
Decay time [ns]			
Fast component	5.0-6.3	2.0	2.2
Slow component	860-1090	80-91	27-34
Relative light yield in fast/slow component			
Fast component	8% (57%)	1%	5% (31%)
Slow component	92% (43%)	99%	95% (69%)
Refractive index at 170 nm	1.29	1.40	1.60

Plastic plates of Polymethylmetacrylate (PMMA) doped with organic scintillator, have been used for electromagnetic and even more extensively for hadronic sampling calorimetry.

The principal difficulty using this technology, is the light extraction. The aspect ratio of scintillator tiles of typically 10cm x 10cm size and 0.5cm thickness would require light guides of typically 10cm x 0.5cm section in order to extract the light while preserving the emission phase space (respecting Liouville's theorem), a very difficult task in realistic detector layouts.

An elegant solution is the use of wavelength shifters in which due to their isotropic emission a stable fraction of the light is transported from the scintillating tile to a small rod, or even a plastic fibre separated from the tile by an air gap.
The wavelength change allows to "violate" the Liouville's theorem

Such a principle is being used by CDF,Atlas TileCal,LHCb Hcal,….
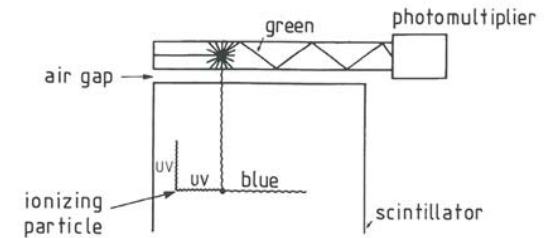

Wavelength shifter readout of a scintillator.

Further development of this technique ,towards detectors capable of accommodating smaller transverse granularities (like 5cmx5cm) were proposed, like the "Shashlik" concept in which readout fibres cross the scintillating tile and the passive converter perpendicularly to their faces (used by LHCb for their ECAL)
Even more ambitious was the "Spaghetti" calorimeter in which each calorimeter cell (typically 1x1 ρ_M transverse size and 25 X_0 deep) is built out of scintillating fibres embedded in a lead matrix ,running parallel to the long side of the block

The concept of APDs was extended to "Silicon Photomultipliers" by dividing the surface exposed to photons into small pixels, in a number large enough that each of them receives at most one photon in a given event..
Operating the device in the Geiger mode (saturated), and summing the current of a large number of pixels, one obtains effectively the equivalent of an analogue response to the number of incident photons, while each pixel operates in a binary way.
Such "miniatures "photon converters are the new key to developing very high granularity scintillatir sampling calorimeters.
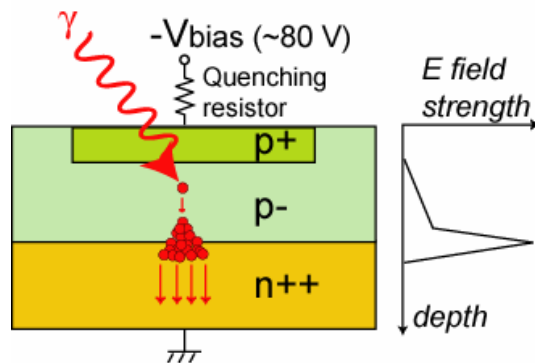
~1000 cells of 25 x 25 microns
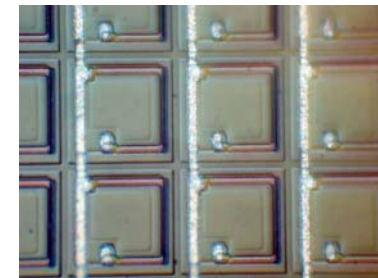
3.2 Cherenkov light collection and conversion

When a charged particle (electron or positron in the case of an electromagnetic shower) propagates in a transparent medium with a speed βc, larger than the speed of light c/n in this medium, an electromagnetic wave forms along a cone of half-angle $\theta_c = \text{Acos}(1/\beta n)$ with respect to the incident particle direction, and with an intensity of emitted photons in the visible range (400 to 700 nm) per unit length:

$$dN/dx = 490 \sin^2\theta_c \; [\text{cm}^{-1}].$$

-Lead glass, a dense material with a high index of refraction, has been used in several experiments (in particular OPAL at LEP) with very similar geometries (tapered bars) as described above for scintillating crystals (Japan was leader for this detector).

-The energy resolution is limited by the number of electrons and positrons in the shower above the Cherenkov threshold, resulting in a stochastic terms $\sigma(E)/E$ of $>\sim 5\text{-}6 \, \%/\sqrt{E}$, comparable to very good sampling calorimeters.

-Readout by photomultipliers is mandatory.

-Response of lead glass to hadronic showers is low (a large fraction of the hadronic cascade is made of non relativistic particles), inducing a performance limitation for hadronic calorimetry behind $\rightarrow$not used when jet calorimetry is important.

-Energy measurement with Cherenkov light produced in water was used with great success in very large detectors for nucleon decay and solar neutrino experiments, like Superkamiokande .

.In Superkamiokande, 50% of the outer surface of the detection volume is covered by 50 cm diameter phototubes. Electrons of 10 MeV are reconstructed with an energy resolution of about 15%. Their position in the detector volume is reconstructed with an accuracy of 70 cm and their direction with an accuracy of ~25 degrees. The detector also provides some discrimination between electrons (showering) and muons (single Cherenkov cone).

3.3 From ionisation to electrical signal in dense materials

Another major avenue for calorimetry is the measurement of the charge created by ionisation in dense, active materials. Under the influence of an applied electric field the charges move, creating a current in readout electrodes proportional to the liberated charge and hence to the energy deposited by the showering particle.

Basic adavantage/scintillation: Electric charges are much easier to transport and to collect than light.

Noble liquid ionisation calorimeters offer a number of attractive advantages, especially for instruments in the difficult environment of colliders. They are characterized by intrinsic stability and excellent uniformity of response (the only amplification is in the easy to calibrate electronics chain), relative ease of a high segmentation and reasonable cost.

Liquid Argon is by far the most used liquid for sampling calorimetry.
The heavier noble liquids (Kr,Xe) have been used for homogeneous calorimetry,given their shorter X0.

. Besides the value of dE/dx and X_0 specific to the material, important parameters are:
- the mean energy needed to create an electron-ion pair
- the electron drift speed as a function of the electric field
- the dielectric constant which affects the capacitance of a readout cell.

Since the ions have a much smaller drift velocity compared to electrons, a track crossing a gap (and depositing charge uniformly) will give rise to a triangular current.

Denoting $+Q_0$ and $-Q_0$ the liberated charges, d the gap, and v the drift velocity of electrons, the resulting current is

$$I(t) = Qv/d$$

with $Q = Q_0 (1-vt/d)$. This formula is easily retrieved by remembering that a point charge q at a distance x from one of the parallel planar electrodes defining the gap of width d, induces a charge $-q(d-x)/d$ on this electrode ,and $-qx/d$ on the other one.
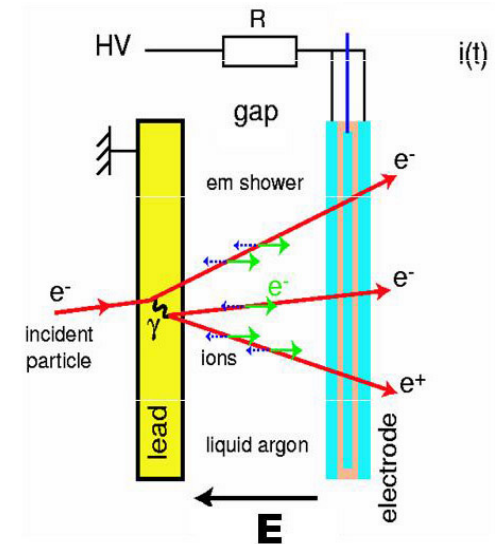
Depending on the particle rate, the readout can be

-an integrated charge readout (which is equal to $Q_0/2$ for uniform charge deposition in the gap)
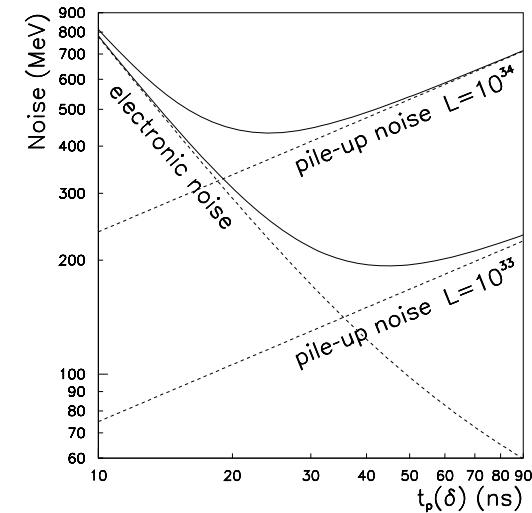
-or a current readout (new since Atlas)

 In the first case the response is rather slow (~400 ns for a 2mm gap in LAr)

 In the latter the response can be much faster (~ 40 ns rise time with a suitable CR-RC2 electronics filtering) but the signal to noise ratio is worse given that less "equivalent "charge is sampled, and the bandwidth of the electronics needs to be larger. At high speed (current readout) the limitation comes from the capacitance and inductance of the elementary readout cell, which must be kept appropriately small.The noise corresponding to pile-up needs also to be included in the overall optimisation
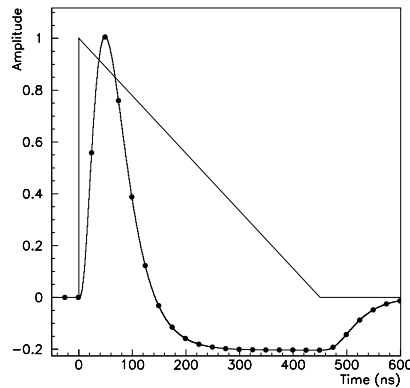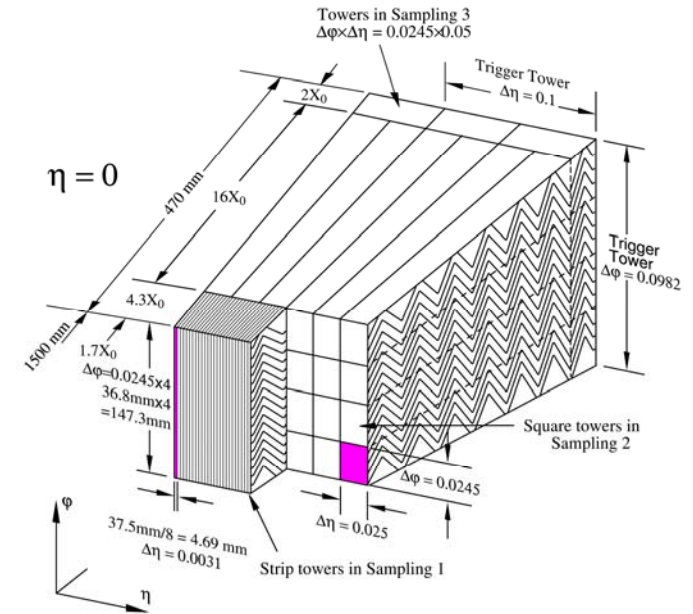

Current from drifting charges (triangle), and after CR-RC2 shaping.
 The dots every 25ns represent times where the signal is being sampled
     (40 MHz sampling like at the LHC)

Optimisation of shaping time between electronics
Noise and pile-up noise

Sketch of the "accordion geometry" which includes 3 samplings in depth.

An important example is the electromagnetic calorimeter for the ATLAS experiment at the LHC which uses an 'accordion' geometry to achieve the LHC performance specifications(fast charge transfer compatible with current readout)
This geometry provides also full azimuthal symmetry without "cracks" between adjacent modules.

Homogeneous noble liquid calorimeters with very high granularity readout can lead to very interesting imaging and energy measurement properties.
One concept, inspired by gaseous tracking chambers (TPCs), was pioneered by the ICARUS collaboration.
Detectors of this type with long drift distances (1m or above) find their application in low rate experiments, such as neutrino experiments.
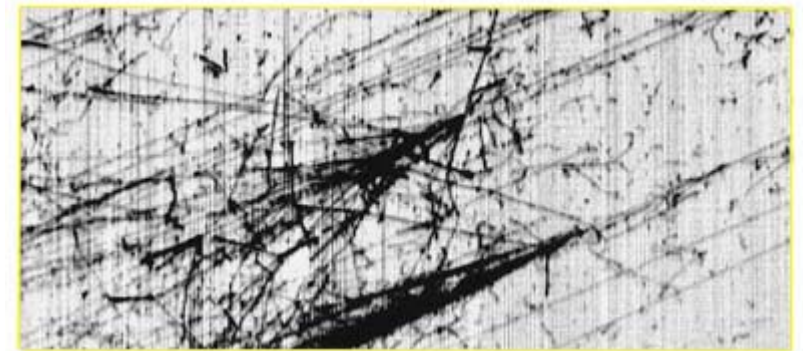
A potentially attractive alternative to noble liquids is the use of fully depleted high resistivity silicon diodes.
The energy to create an electron-hole pair is about 10 times smaller than in noble liquids,and the electron drift speed is higher.
Problem: high cost→limited so far to small devices,like the luminosity calorimeter of the Aleph experiment at LEP:
-two-arm detector, located at +- 2.5 m from the collision point, covered the polar angles from 24 to 58 mrad.
-Consisted of a stack of 12 layers of silicon sensors interleaved with tungsten absorber plates, for a total thickness of ~24X_0

-High resistivity, n-type (7kΩ-cm, 300μm thickness) Si was used for the 1.3 m^2 readout area, divided into 12 228 channels.
-Noise ~ 0.13 mip, for a signal peaking time of 250ns.

In order to fully exploit the physics potential of a future e$^+$e – Linear Collider, with Centre of Mass energy up to several hundreds of GeV, electromagnetic calorimeters with extreme granularity (up to 100 million channels) are being considered.
Silicon diodes coupled to microelectronics readout are the only feasible solution for this approach.

3.4 Gas amplification

Charge collection in (mixtures) of noble gases followed by some degree of internal amplification (wires, GEMs, micromegas, RPCs…) forms the basis of another important category of ionisation sampling calorimetry.
Lends itself naturally to highly segmented construction
The low density has several negative consequences:
-Landau-fluctuations of the energy deposit
-low-energy shower-electrons may multiple-scatter into the readout planes, where they may travel distances large compared to the gap thickness of the active layer, resulting in path-length fluctuations.
-As illustration: the electromagnetic calorimeter of the Aleph experiment at LEP
-segmented into 74000 towers.
- energy resolution was measured to be $\sigma(E)/E = 0.18/\sqrt{E} \oplus 1.9\%$ with E expressed in GeV (due to internal amplification, the electronics noise term was negligible).
- weak points of the technique = non-linearity of response.
- test beams → $E_{corr} = E_{raw}(1+0.00078\ E_{raw}(GeV))$ implying a 7.8% correction at 100 GeV.
Such non-linearities affect in particular high energy jets in which several showers may be superimposed, thus affecting the result in a way difficult to correct.
Still adequate at LEP, but electromagnetic gas calorimeters are no longer being considered for higher energy colliders.

3.5 High rate effects and radiation damage

Radiation damage needs to be considered for the active readout material and signal processing electronics .

Calorimeters with gaseous readout are particularly vulnerable to the high radiation environment due to the ageing effects associated with internal gas amplification (polymerisation along wires)

Radiation damage is essentially absent in noble liquids $\rightarrow$ one of the most intrinsically radiation-hard techniques.

However,a rate limitation comes from space charge effects due to the low drift speed of the positive ions (typically in the range of few cm/s at a nominal electric field around 1 kV/mm). At high incident rates these ions form locally a charged domain which effectively shields the electrons in the gap.

Effects are inversely proportional to the square of the operating gap.

For this reason the forward calorimeters of the ATLAS experiment features gaps down to 250 μm.

Scintillators suffer from the formation of colour centres which absorb part of the emitted light.

The qualification of $PbWO_4$ crystals as a candidate for the CMS crystals calorimeter at the LHC required a world-wide R&D program to study the radiation damage effects and to develop methods to avoid them during the crystal growth.

Several impurities were identified to affect transparency in the useful wavelength range (above 350 nm). The best radiation resistance was obtained for crystals grown in Pb/W stoechiometric conditions, with the addition of a small quantity (~100ppm) of Nb and Y . These crystals show a light loss of ~ 5% after an exposure to ~10 Gy in ~10 hours, typical of the radiation fluence for calorimeters at LHC nominal luminosity. These colour centres show annealing with a recovery time of ~10 hours.

Radiation effect on the light transducers (APD) and the front-end electronics need also be considered.

3.6 Calibration and monitoring of calorimeters response

In general, the following tasks have to be performed:

- establishing the absolute scale of response of a calorimeter, averaged over an entire data set.
- assessing the uniformity and linearity of response of a calorimeter
- monitoring the response as a function of time, locally and globally, in order to correct
 for time dependant effects, rate effects, aging.

Invariant mass of two photons in $B\bar{B}$ events recorded in Babar.
    The position of the π^0 peak provides the reference for the energy scale
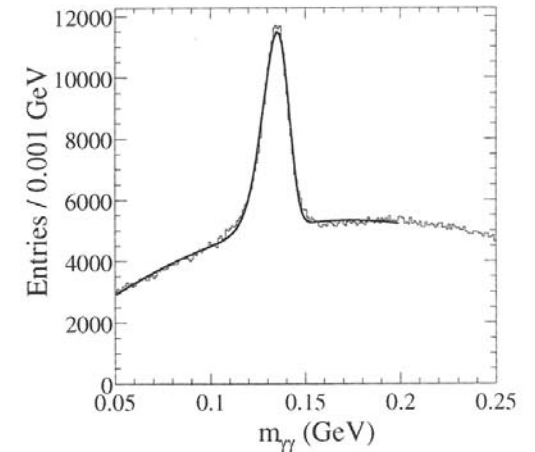
a) Energy scale

 medium energy domain: one example is the Babar/Belle experiments which used CsI crystal electromagnetic calorimeters and employed several calibration sources to cover the full energy range :
    - at the high energy end(~10 GeV) the Bhabha scattering was used.
     (With a luminosity of 3×10^{33} cm^{-2} s^{-1} this reaction provided about 200 events per crystal in a 12 hours run)
    - at the lower end,the peak position of the π^0 in the $\gamma\gamma$ spectrum was adjusted to 135.1 MeV .

high energy domain:
At the Tevatron (2TeV centre of mass) and the
LHC(so far 7TeV in the centre of mass)the energy scale of the
electromagnetic calorimeters is set using the precisely known
mass of the Z^0 (M_Z = 91188 ± 2 MeV) decaying into e^+e^- pairs.

thanks to the increased (factor>10) cross-section of Z^0 production
(Including acceptance and efficiencies, about 8 000 reconstructed
decays in e^+e^- were recorded in Atlas or CMS for the 40pb^{-1} run in 2010).

The high-precision scale is essential for precision measurements
of the W mass using decays in ev.

W bosons decaying into two jets (e.g. isolated jets from top decays)
will be used for jet energy calibration, however with a more modest
(~1%) goal.
An interesting way of getting clean samples of two jets resulting
from a W decay is to use ttbar events, identified by the semi-leptonic
decay of the other W, as well as by displaced vertices signing one
or two of the b decays present in the event.
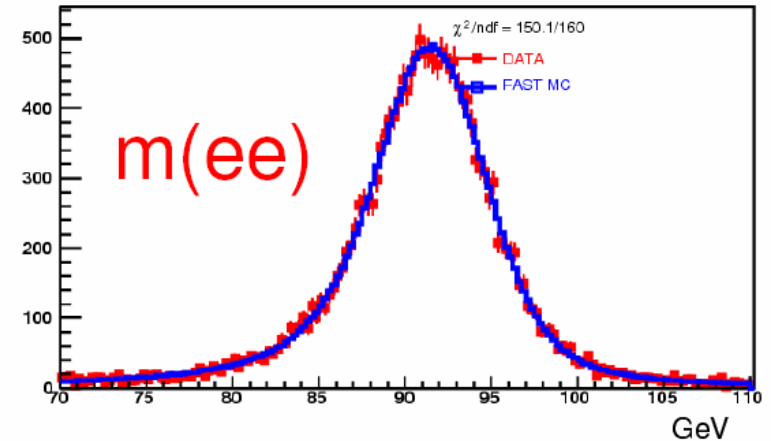
D0 mass spectrum of e+e- events
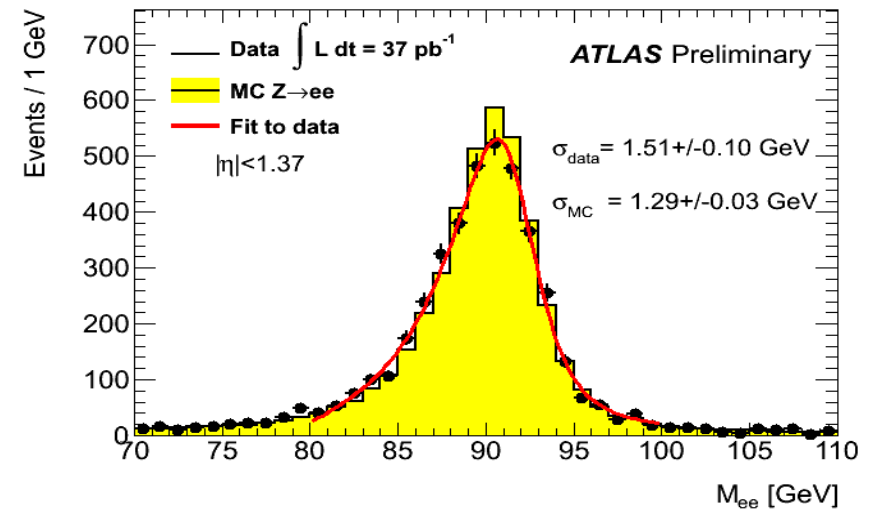
b) Uniformity and linearity

With large enough statistics, the Z^0 mass constraint can be used to rescale in situ the response of a calorimeter sector by sector and to improve its uniformity of response.
.

E/p method   ask E(calorimeter)= p(magnetic spectrometer in front)

   -Works only if the spectrometer material (Inner detector for collider
   Experiments) is low enough
    -used with success in the NA48 experiment(Liquid krypton calorimeter
for CP violation experiment in K decays at CERN).
with a large sample of Ke$_3$ decays, demonstrating a linearity of better than
$\pm 5 \times 10^{-4}$ between 10 and 80 GeV.
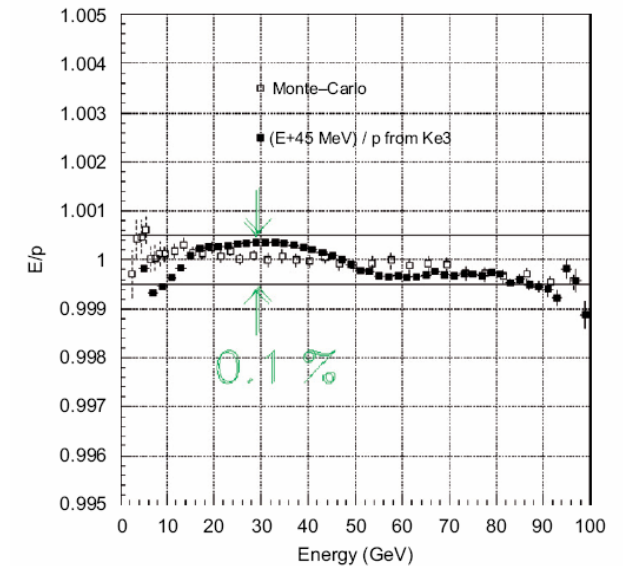
Linearity of the NA48
homogeneous krypton
Calorimeter.

c) Monitoring of short term irradiation effects

In some cases the calorimeter response is subject to time dependant effects,
on a time scale too short to allow for correction with the recorded physics
data itself.
External monitoring is in this case necessary.
An example is the laser monitoring of the CMS crystal calorimeter designed
to follow the light absorption and recovery as a function of the instantaneous luminosity .
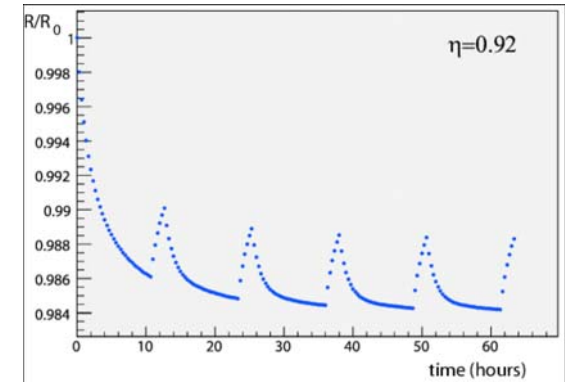
e)Other effects to be monitored:

-Example: the energy response of the ATLAS liquid argon calorimeter depends on the temperature of the liquid bath with a coefficient of -2% per degree. Precision thermometers (Pt 100 platinum resistances) are used to follow the temperature to a precision better than 50 mK.

In all precision experiments the behaviour (gain) of the front-end electronics is monitored by injecting precision electrical pulses, allowing subsequent corrections to be made,with a precision down to 10^{-3} or better.

4 Auxiliary Measurements

4.1 Position and angular measurements

Use energy weighted barycentre of energy deposition.

Examples:

-NA48 (ionisation,homogeneous,2 x 2cm cells) $\sigma_{x,y} = (4.2 /\sqrt{E(GeV)} \oplus 0.6)$mm

- Babar CsI crystal calorimeter (4 x 4 cm crystals) $= 3.2$mm$/\sqrt{E}$ (smaller Moliere radius,less/no noise)

With more than two samplings in depth the direction of photons showers can then be estimated

The Atlas EM calorimeter has three longitudinal samplings →direction of photons with an accuracy of about 60 mr$/\sqrt{E}$

An important asset for the search for the Higgs boson in the low masse region, using the two photon final state.: At high luminosity when there are up to ~20 collisions per bunch crossing the vertex of the candidate Higgs cannot be found from the associated charged tracks.Without precise knowledge of the vertex the mass resolution is significantly worsened

Search for new long lived neutral particles decaying into photons (like neutralino→photon+gravitino in GMSB) also benefit from a high-resolution angular measurement.

4.2 Timing

Time measurement requires additional signal processing. Constant fraction discriminators or digital treatment of multiple samplings of the signal (also beneficial for energy measurements)are frequently used. The shaping time of the electronics is a critical parameter in optimizing the timing accuracy.

NA48 krypton calorimeter showed a resolution of $\sigma = 0.5$ ns$/\sqrt{(E)}$, up to ~100 GeV.

MEG experiment at PSI(see later) gives ~100ps for 50 MeV photons in liquid krypton(light readout)

CMS and Atlas calorimeters can achieve ~100ps as well,but for energies> 50 GeV or so

With a time resolution better than 100ps (ie 3cm) vertex constraints for neutral particles become accessible.

4.3 Electron and photon identification

Criteria used are ;
-shower shape (much narrower for EM shower)
-no energy in the hadronic compartment
-further rejection of π^0 if high granularity in the front compartment can distinguish the 2 photons of the decay(Atlas)
As an illustrative figure, simulations made for the ATLAS experiment, give a rejection factor of jets of about 3000 (for a photon acceptance of 80%),when studying the γ+jet final state as a possible background to the $\gamma\gamma$ reaction, with photon p_T around 50 GeV/c.
For certain physics reactions an 'isolation criterion'-absence of tracks above a certain p_T ,nor calorimeter energy in a cone around the electromagnetic shower- can be applied to sharpen photon or electron identification. This criterion does not apply e.g. for electrons resulting from heavy quark decays, inside the heavy quark jet.

5 Jets and Missing Energy

Jets and the related signature of 'Missing Energy' have contributed to major discoveries (gluon, W-boson, top quark,..).
At LHC they will provide key signatures, e.g. for SUSY studies.

The measured jet energy has to be related to the corresponding parton (quark, gluon) energy in sequence of complex steps. Initial and final state gluon radiation and parton fragmentation affect the observable particle composition and momenta in the jet, limiting the 'intrinsic' parton energy resolution to order $\sigma(E_{parton})/ E \approx$ $0.5/\sqrt{E_{parton}}(GeV^{-1/2})$
. Experimental factors – different response as a function of particle species and momentum, nonlinearities, insensitive detector areas, signal noise, magnetic field – require large corrections.

The jet energy scale can be experimentally validated by:

- Studying specific final states in which the jet is balanced by a well measured object, such as γ + Jets(s) or Z + jet(s).

- Another powerful constraint is provided when a sample of W's decaying into two jets can be isolated.

The measurement of 'Missing Transverse Energy' is the only way to infer the production of neutrinos or weakly interacting SUSY-type particles.

It is defined as the negative vector sum of all energy deposits projected onto the plane transverse to the collision direction. Empirically, a missing energy resolution of $\sigma (E_{missing}) / E \approx 0.7\ \alpha\ /\sqrt{\sum E_{Tparticles}}$ (GeV$^{-1/2}$) is observed for soft collisions, where the sum is over all particles in the acceptance and α is again the stochastic term for single hadron resolution.

However, calorimetric systems with an acceptance of at least |η| > 5 and very good 'hermeticity' are required to achieve this performance→This has been a very strong constraint on the design of LHC experiments.

The forward region is the place where most energy from collisions (boost factor)is deposited → radiation damage
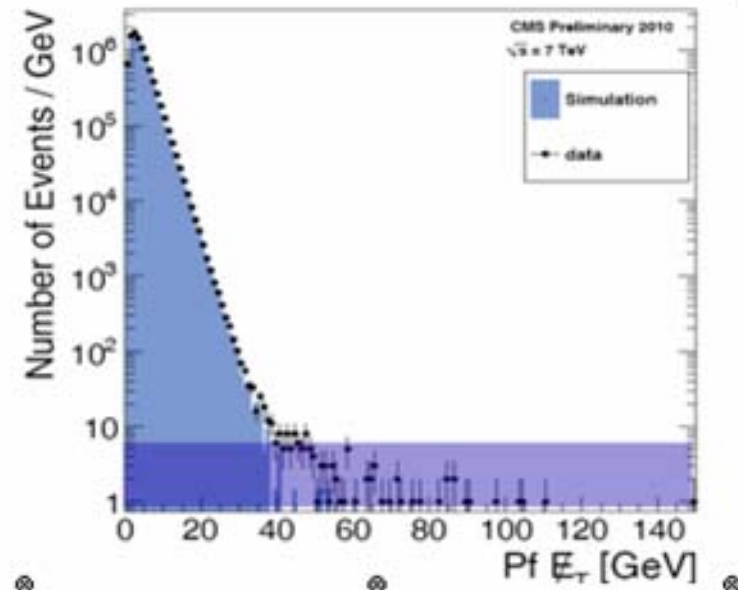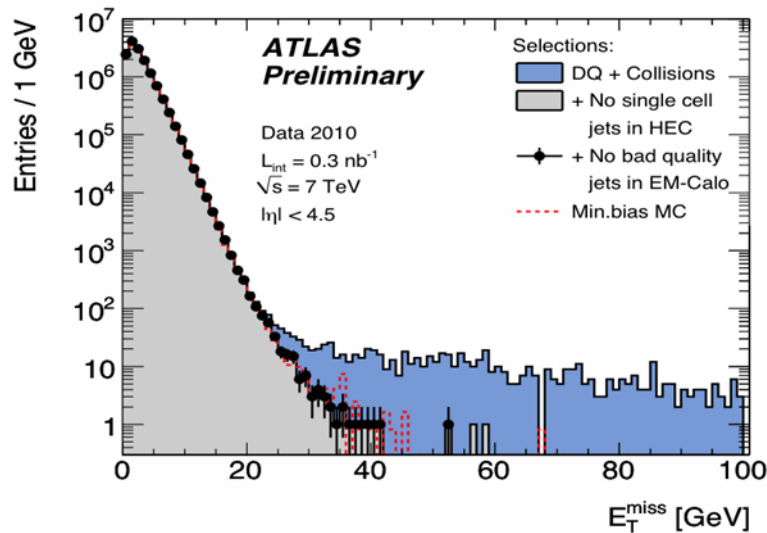
Missing transverse energy in ATLAS(left) and CMS(right) minimu bias events at 7 TeV Cenetr of mass energy

6 Triggering with calorimeters

The ability of calorimeters to provide rapidly (order 100 ns) information on the energy distribution of the collisions products is one of the major attractions of this technique.

It provides a selectivity of $\sim 10^{-3}$ and reduces the 10^{9}/sec collisions rate accordingly. A 'Sliding Window' technique is used to search for local energy topologies in $\Delta\eta \times \Delta\varphi$ transverse energy distribution.

The optimum window size depends on the particle type (photons, electrons or hadrons), on the jets, their threshold, the depth of the calorimeter included in the sum and possibly luminosity. More complex topologies requiring isolated energy clusters (e.g. triggering on isolated photons or electrons) are also used.

The L1 trigger is implemented with dedicated hardware processors.

In subsequent stages (L2, L3) selection criteria and energy thresholds are sharpened with software-based algorithms.
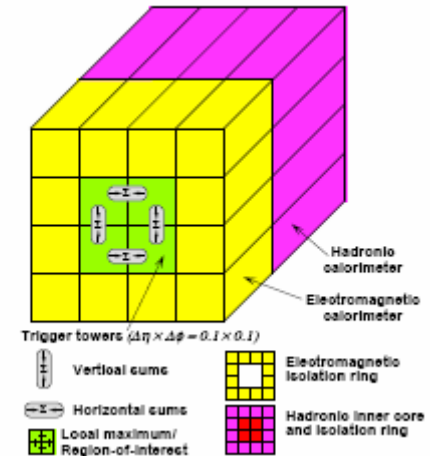
7 Examples of Calorimeters and Calorimeter Facilities

Electromagnetic Calorimeters

7.1 The MEG Noble Liquid homogeneous calorimeter with light readout

. The MEG experiment at PSI is dedicated to the search for lepton flavour
violation in muon decays at rest.
It aims at a sensitivity for $\mu \rightarrow e\gamma$ decays of 10^{-13} after 2 years of running.
This requires an outstanding background rejection (for example of the reaction $\mu \rightarrow e\nu\nu\gamma$)
and thus call for a calorimeter with an excellent energy resolution for ~50MeV photons,
and a sub-ns response to cope with the high rate.
The calorimeter has a half-cylinder shape.
It contains 800 litres of liquid Xenon, and is readout by PMTs with K-Cs-Sb photocathodes and
Silica entrance windows transparent to the peak of light emission (175 nm) of liquid Xenon.
Approximately 30% of the outside surface of the detector volume is covered with 846 PMTs.
The detector is optimised for events with a single photon shower in the volume.

High purity (at the ppb level) of the liquid is necessary to prevent UV photons for being
absorbed by contaminants like oxygen and water.
. The PMT signals are digitized at 2 GHz with a 12 bit accuracy using custom designed electronics.
The energy scale of the calorimeter(particularly important for the end-point spectrum) is calibrated with photons (17.6 MeV) from
the $Li(p,\gamma)Be$ reaction obtained by sending protons from a Cockroft-Walton source to a Li target close to the calorimeter.
The relative energy resolution (rms) found at 50 MeV is 2.3 % .The position resolution is ~6mm and the timing resolution 64 ps.
These excellent results, made possible with this innovative technique, match the demanding requirements of the experiment.
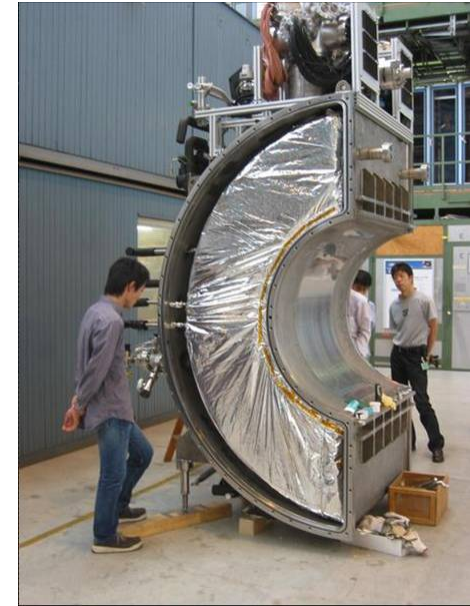
7.2 The CMS electromagnetic Crystal Calorimeter

The largest crystal calorimeter assembled so far is the $PbW0_4$ calorimeter of the CMS experiment at the CERN LHC clearly aimed at the Higgs -> $\gamma\gamma$ discovery.

Cylindrical barrel part (inner radius ~1.3m) and two end-caps at about 3m from the proton-proton collision point .

Each of the 61200 barrel crystals is a tapered bar ($\Delta\phi$ x $\Delta\eta$ = 0.018 x 0.018) and has a depth of 23 cm (24.7 X_0).

In the end-caps, the calorimeter is preceded by a lead-Silicon strips preshower.

The calorimeter is located inside the hadronic calorimeter, which in turn is inside the 3.8 T superconductiong solenoid.

Barrel crystals are readout by APDs(insensitive to magnetic field) while the endcap crystals (somewhat bigger) are readout by phototriodes chosen for their better radiation resistance.

The equivalent noise per crystal is ~ 30 MeV.

Layout of the CMS electromagnetic calorimeter,
showing the arrangement of crystals,with the preshower
in front of the end-caps
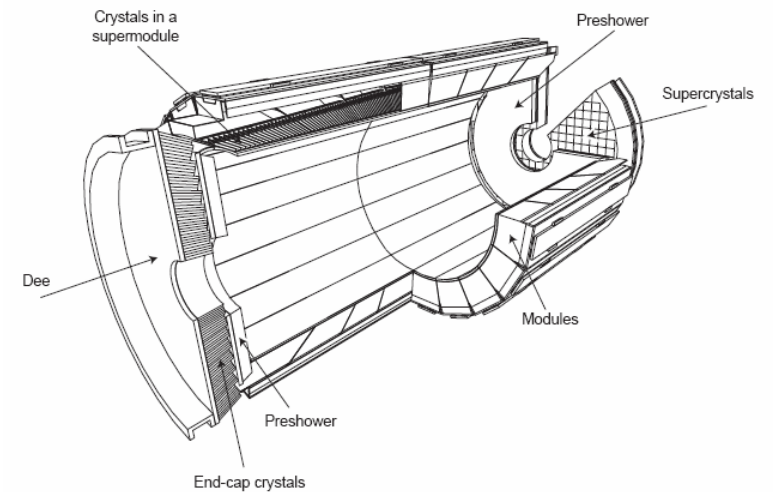
Initial Calibration: all barrel modules were exposed to cosmic muons at ground level, with a statistics of about 100 muons (aligned with the crystal axis) per crystal.

Test beam and cosmics calibration agree at the level of ~ 1.5%

Based on the test beam data the relative accuracy (rms) of the energy reconstruction of photons in a 5 x 5 cluster is estimated to be 0.5% at 120 GeV(Important asset for Higgs search in two photons)

For electrons this excellent performance will be affected by their radiation in the inner detector material (up to ~1X_0)

7.3 The ATLAS 'accordion' electromagnetic calorimeter.

The electromagnetic calorimeter uses a lead/liquid argon sampling technique, with an 'accordion' geometry, and is located outside of the inner solenoid.

Liquid argon was chosen for its immunity to radiations, its intrinsic stability and linearity of response, and its relative ease for longitudinal and transverse segmentation.

Its more modest intrinsic energy resolution (σ(E)/E = 10%/$\sqrt{E}$ $\oplus$ 0.25/E $\oplus$ 0.003 from test beams) is a limiting factor at medium and low energies.

The calorimeter features three segments in depth, the first one having an extremely fine segmentation in pseudorapidity (0.003) to allow separation between prompt photons and photons from π^0 decays up to p_T ~70 GeV/c, the interesting range for the Higgs boson search in the $\gamma\gamma$ decay mode.

The calorimeter is preceded by a presampler, in the same cryostat, to correct for the loss of energy of electrons and converted photons in the upstream material.

The barrel part, consisting of two cylinders and of the two endcap wheels provide fully uniform azimuthal "crackless" coverage despite being built of 16(8) modules per cylinder (wheel)

The font-ectronics shaping was optimized for best performance at the nominal LHC luminosity of $10^{34} cm^{-2}s^{-1}$.

The dynamic range is covered with three gain channels in the ratio 1/9/81, digitized with 12 bit resolution.

Trigger towers of size $\Delta\eta$ x $\Delta\varphi$ = 0.1 x 0.1 are built by analogue summing of signals at the front-end level ollowed by digitization at 40 MHz with 10 bits ADCs (sensitivity of 1 GeV per count).

The uniformity of response within one module and the reproducibility from module to module were checked in a test beam.

An overall dispersion of energy measurements in 3 barrel modules and 3 end-cap modules was respectively 0.43% and 0.62%

The energy scale and the long range uniformity will be assessed in situ using the Z mass constraint
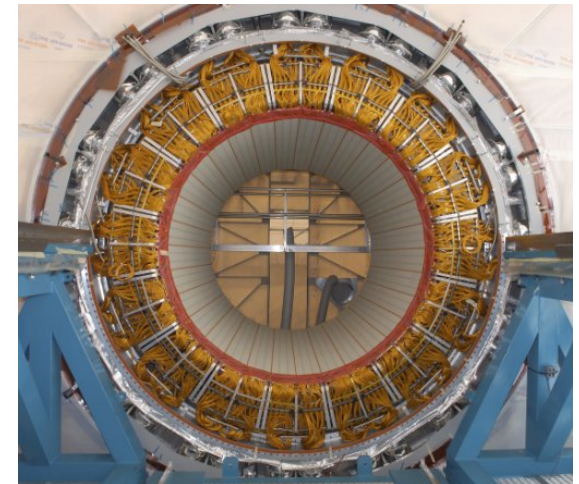
Hadronic Calorimeters

7.4 The ZEUS calorimeter at HERA

Research at the electron-proton collider HERA required precision jet spectroscopy at the 100 GeV level to study the underlying dynamics of e–quark collisions.

H1 calorimeter based on the LAr-Pb and LAr-Fe sampling technology. A certain level of 'off-line' compensation was achieved because hadron showers were measured longitudinally up to ten times and longitudinal shower-weighting could be applied

ZEUS calorimeter based on the U-scintillator sampling technique. The ratio of the thickness of the ^{238}U plates (3.3 mm) to the scintillator plates (2.6 mm) was tuned to achieve e/π = 1, confirmed by measurements to be e/π = 1.00 ± 0.03.

The measured hadronic energy resolution, σ/E (hadrons) = 0.35/$\sqrt{E(GeV)}$ is consistent with a sampling resolution of σ/E (sampling, hadrons) ≈ 0.29/$\sqrt{E(GeV)}$ and an intrinsic resolution of σ/E (intrinsic, hadrons) ≈ 0.20/$\sqrt{E(GeV)}$.

This sampling frequency is rather coarse for electrons resulting in an electron energy resolution σ/E (electrons) = 0.18/$\sqrt{E(GeV)}$.
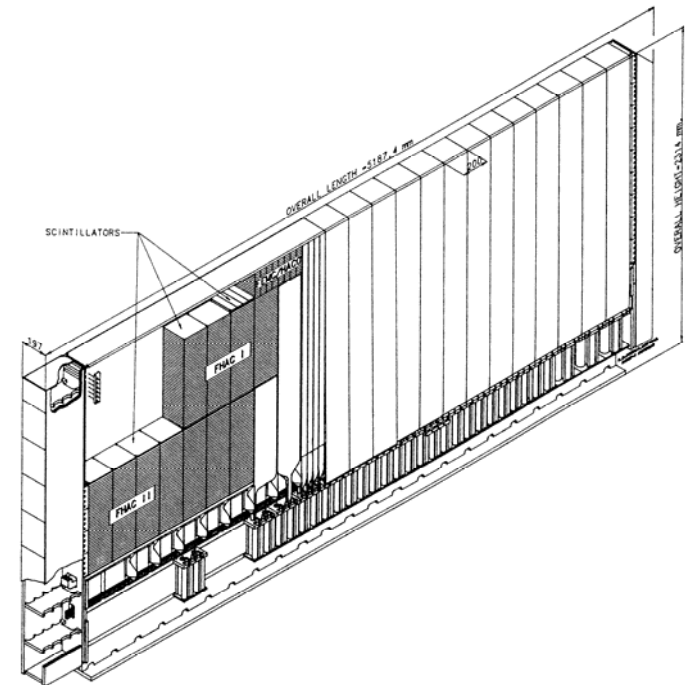
View of a module of the ZEUS U-scintillator calorimeter. Wavelength-shifter readout is used to read cells of 5*20 cm^2 cross-section in the electromagnetic compartment and of 20*20 cm^2 in the two subsequent hadronic compartments

Facilities at LHC

7.5 In ATLAS the 'Accordion' calorimeter is followed in the barrel by a hadronic Fe-scintillator tile / WLS fibre readout.
- The unconventional geometry of absorber plates and scintillating tiles oriented along the direction of the incident particle permits an economic construction and homogeneous sensitivity .

Pion resolution in test beams: $\sigma/E \approx (0.52/\sqrt{E} \oplus 0.03/E) \oplus 1.6/E$ (LAr + Tile)

Estimated jet energy resolution of $\sigma(jet)/E \approx 0.6/\sqrt{E(GeV)}$

- For the 'endcap' regions ($1.4<\eta<3.2$) ATLAS had to adopt different solutions to cope with the radiation levels.

An Accordion-type electromagnetic calorimeter precedes a Cu/Liquid Argon hadron calorimeter.

In the very forward region ($3<\eta<5$) yet another novel geometry had to be invented: cylindrical readout elements with narrow LAr-gaps (0.25 to 0.35 mm) as sensitive medium are embedded in a tungsten absorber, sampling geometrically very tight showers at adequate readout speeds.

ATLAS

7.6 CMS

Compact Muon Solenoid
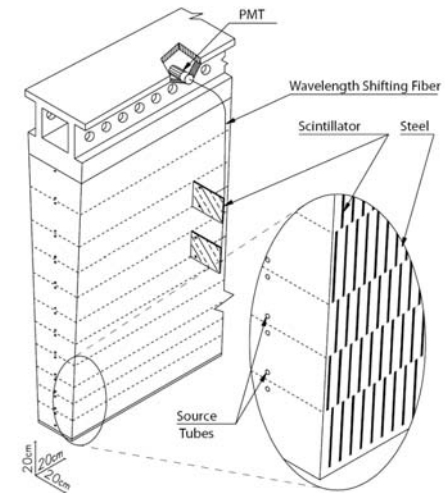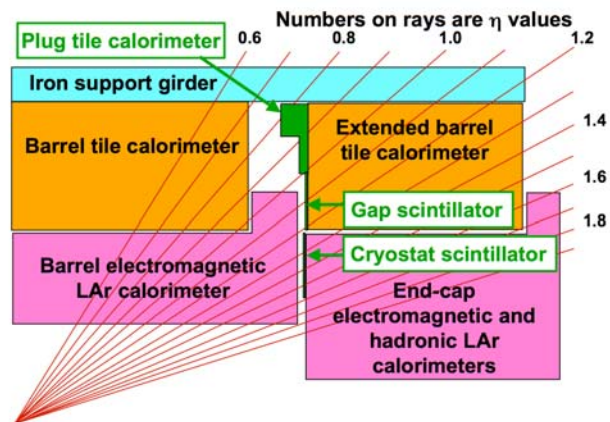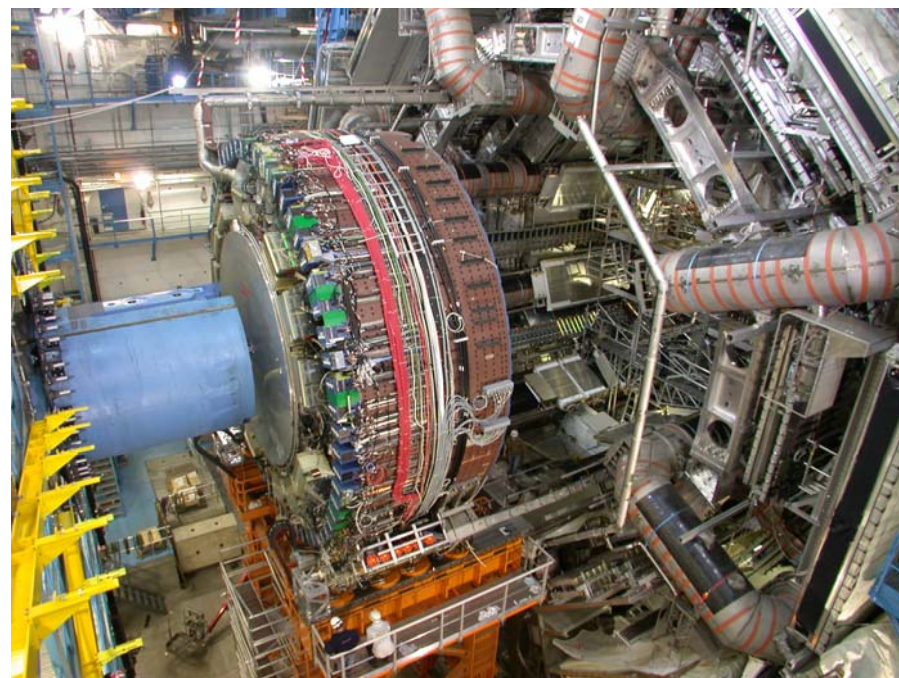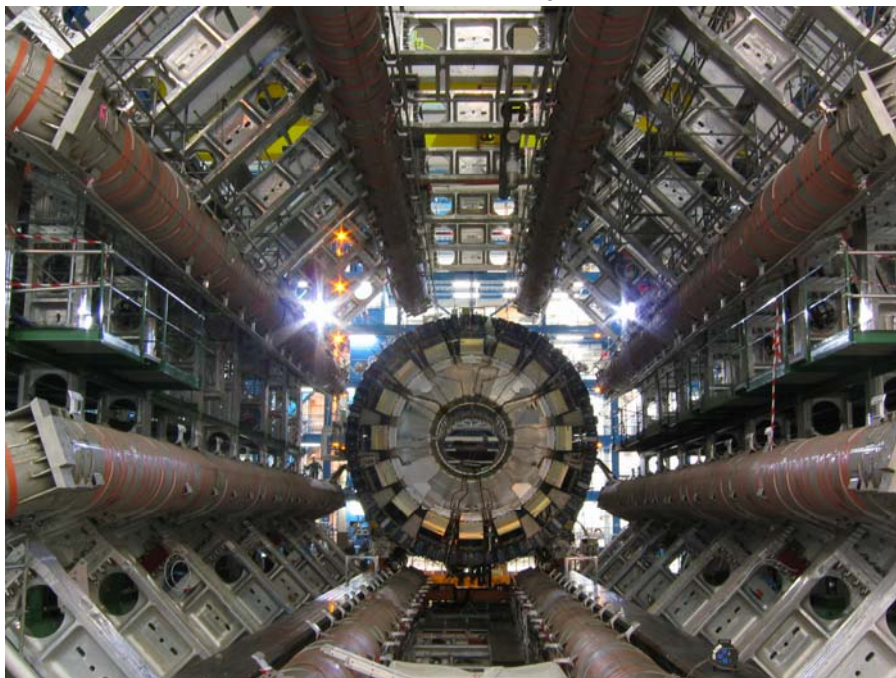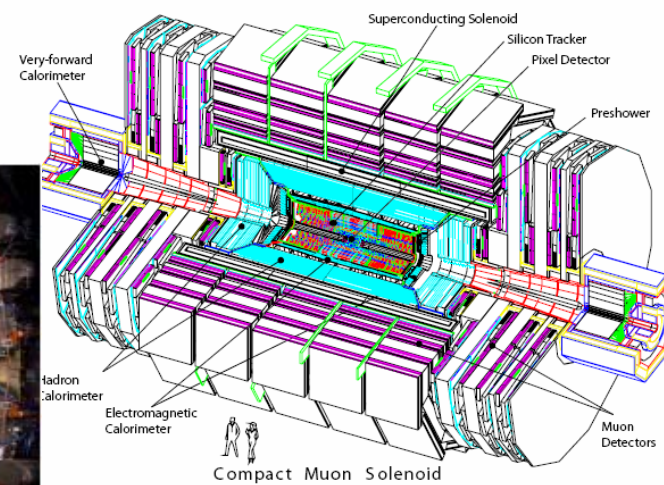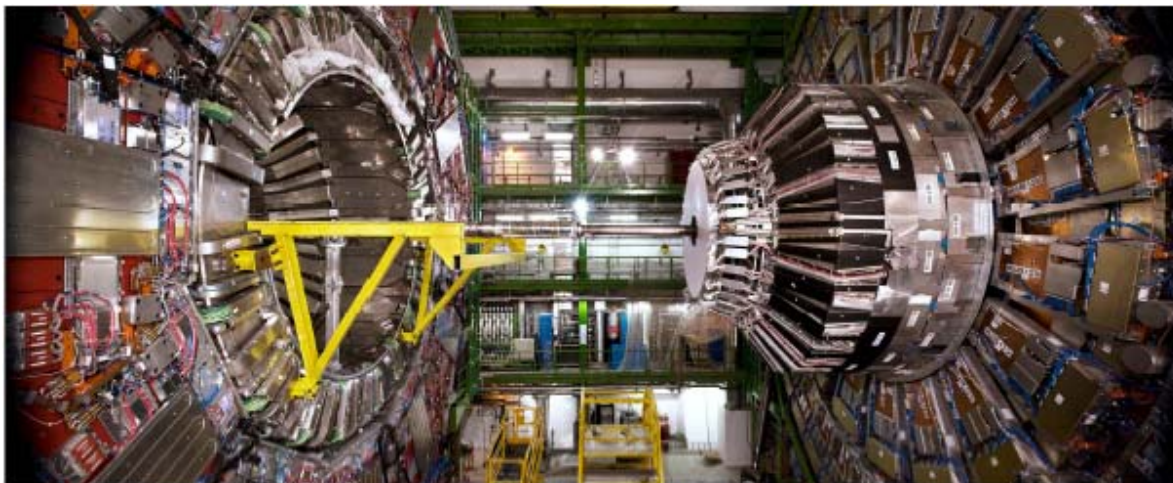
CMS uses:
-brass-scintillator readout by wavelength shifter in the barrel and endcaps,and
-Fe-quartz fibers (Cerenkov) in the very forward direction

7.7 Developments for Linear Collider calorimetry

Physics emphasis put on tracking and jets (and taus)
The LC jet benchmark resolution is $\sigma/E \approx 0.30/\sqrt{E}$

Two directions of R&D are being followed:

- 'Particle Flow Analysis': using
  -the inner detector to measure charged particles,
  -only neutrals(mainly π^0 and photons) for the EM calorimeter part
  -and neutrons and KL for the downstream hadronic calorimeter part.
     The difficulty is to unfold the showers associated to these neutrals
from those produced by the charged ones
          $\rightarrow$high granularity is emphasized
   Silicon diodes interleaved with W plates are the first choice at present stage of R&D (Calice Collaboration,US SiD)

- Dual REAdout Method
 Aim at separating, tower by tower, the electromagnetic component through Cherenkov light and the hadronic component through scintillation light.
  Wavelength filtering might provide an additional handle to disentangle the various processes,as well as timing (e.g. delayed nuclear photon emission).
  The combined information could in principle allow complete reconstruction of the shower- and jet composition.
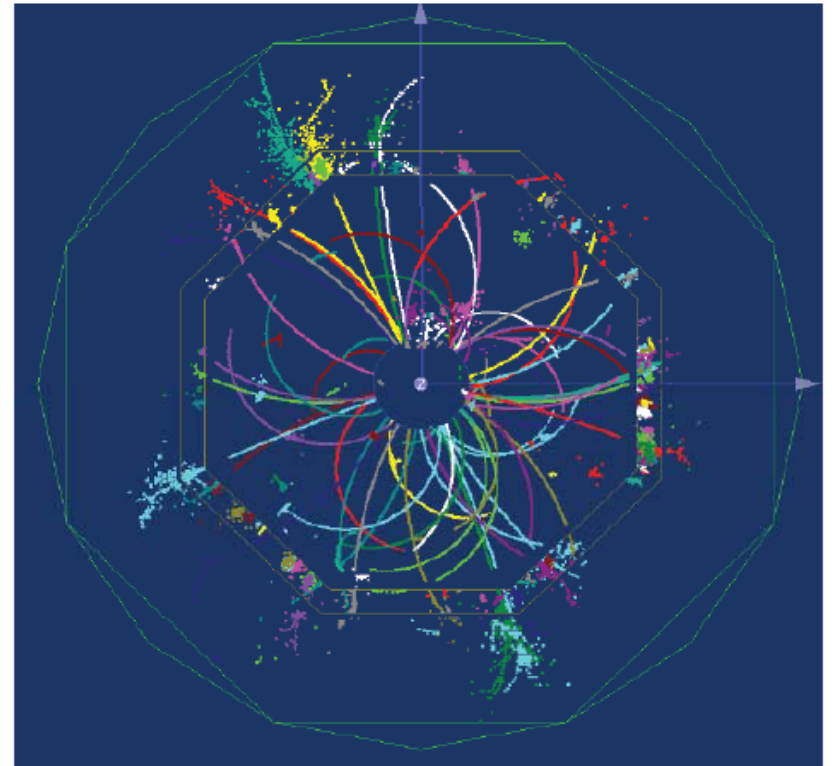
CONCLUSIONS

- <u>Electromagnetic calorimetry</u> has matured into a precision measurement technique,with energy accuracy below 1%, and several additionnal functions (timing,position,…). It was and is presently a key element in precision experiments (NA48,MEG,…) as well as in general facilities at the B-factories,Tevatron and now LHC

- <u>Hadronic calorimetery</u> has been present, and a key element in general facilities at   HERA, Tevatron and the LHC.

Better understanding of the basic hadronic processes at work,as well as exploitation of various sources of signals (scintillation, Cerenkov ,delayed neutrons) can still lead to significant improvement in performances.

Clever combination of tracking and calorimetry may lead to substantial improvements in Jet spectroscopy, for example at the future ILC or CLIC.

……..As a recommendation to young generation: you have to know which physics you want to address before investing your time in detector developments, and vice-versa ,you have to understand in detail the (in general complex) behaviour of the detector in order to extract from it meaningful physics results.

Appendix:

Parameters of the ATLAS and CMS electromagnetic calorimeter facilities

	Atlas		CMS	
Technology	Lead/Lar accordion		PbWO4 scintillating crystals	
	Barrel	**Endcaps**	**Barrel**	**Endcaps**
η coverage	0-1.475	1.4-3.2	0-1.48	1.48-3
channels	110208	63744	61200	14648
Granularity	ΔηxΔ		ΔηxΔ	
Pre-sampler	0.025x0.1	0.025x0.1	-	-
Strips/Si-preshower	0.003x0.1	0.003-0.006x0.1	-	32x32 Si-Strips Per 4 crystals
Main sampling	0.025x0.025	0.025x0.025	0.017x0.017	0.018x0.003 To 0.088x0.015
Back	0.05x0.025	0.05x0.025	-	-
Depth				
Pre-ampler	10 mm	2x2 mm	-	-
Strips/Si-preshower	~4.3Xo	~4.0 Xo	-	~3 Xo
Main sampling	~16 Xo	~20 Xo	26 Xo	25 Xo
Back	~2 Xo	~2 Xo	-	-
Energy Resolution				
Stochastic Term	10%	10-12%	3%	5.50%
Local constant term	0.20%	0.35%	0.50%	0.50%
Noise per cluster (MeV)	250	250	200	550

Parameters of the Atlas and CMS hadronic calorimeter facilities

	ATLAS	CMS
Technology [η half-coverage]		
Barrel / Ext. Barrel	14 mm Fe / 3 mm scint [0- 1.4]	50 mm brass / 4 mm scint. [0- 1.4]
End-caps	25 mm (front) – 50 mm (back) Cu/ 8.5 mm LAr [1.4 -3.2]	80 mm brass/ 4 mm scint [1.4 – 3.0]
Forward	Cu (front) – W (back)/ 025 – 0.50 mm LAr [3.2 - 4.9]	4.4 mm steel / 0.6 mm quartz [3.0 – 5.0]
Channels		
Barrel / Ext. Barrel	9852	2592
End-caps	5632	2592
Forward	3524	1728
Granularity (Δη x Δφ)		
Barrel / Ext. Barrel	0.1 x 0.1 to 0.2 x 0.1	0.087 x 0.087
End-caps	0.1 x 0.1 to 0.2 x 0.2	0.087 x 0.087 to 0.35 x 0.028
Forward	0.2 x 0.2	0.175 x 0.175
Longitudinal Samplings		
Barrel / Ext. Barrel	Three	One
End-caps	Four	Two
Forward	Three	Two
Absorption lenghts		
Barrel / Ext. Barrel	9.7 – 13.0	5.8 – 10.3 10 – 14 (with Coil / HO)
End-caps	9.7 – 12.5	9.0 – 10.0
Forward	9.5 – 10.5	9.8